Characterization and Circuit Modeling of Electromagnetic Interference Filtering Chokes in Power Electronics: A Review

Huamin Jie, *Graduate Student Member, IEEE*, Zhenyu Zhao, *Senior Member, IEEE*, Hong Li, *Senior Member, IEEE*, Changdong Wang, *Member, IEEE*, Yongqi Chang, *Graduate Student Member, IEEE*, and Kye Yak See, *Senior Member, IEEE*

***Abstract*—With the evolution of Industry 4.0 and the surge in demand for sustainable energy, power electronics are becoming essential in various applications. Considering the reliability and safety of power electronics devices, studying and addressing the conducted electromagnetic interference (EMI) issues are of paramount importance. Due to the merits of versatility, flexibility, and effectiveness, passive filters containing EMI filtering chokes and capacitors are commonly used. Among them, EMI filtering chokes have been widely investigated in recent years because they account for most of the weight and size of a passive filter and mitigate considerable EMI noises. To the best of our knowledge, this article presents the first review of EMI filtering chokes used in power electronics that specifically focuses on their characterization and circuit modeling. These topics help to evaluate choke performance, optimize choke configuration, and facilitate systematic simulation, ultimately refining filtering design. Starting with an overview, the type, structure, principles, information, and modes of chokes are demonstrated. For choke characterization, various analytical, numerical, and measurement methods are compared. Using the characterized information, their distributed, lumped, and multistage circuit models along with the relevant parameterization process are summarized. Finally, existing challenges, ongoing innovations, and future topics are explored.**

***Index Terms*—Choke characterization and circuit modeling, electromagnetic interference (EMI), EMI filtering chokes, power electronics.**

Received 16 April 2024; revised 18 June 2024 and 18 July 2024; accepted 31 August 2024. Date of publication 3 September 2024; date of current version 12 December 2024. This work was supported in part by the Nanyang Technological University, National University of Singapore, and in part by the National Science Fund for Distinguished Young Scholars of China under Grant 52325704. Recommended for publication by Associate Editor F. Dijkhuizen. *(Corresponding author: Zhenyu Zhao.)*

Huamin Jie and Kye Yak See are with the School of Electrical and Electronic Engineering, Nanyang Technological University, Singapore 639798 (e-mail: jieh0002@e.ntu.edu.sg; ekysee@ntu.edu.sg).

Zhenyu Zhao is with the Department of Electrical and Computer Engineering, National University of Singapore, Singapore 117583 (e-mail: zhaozy@nus.edu.sg).

Hong Li is with the College of Electrical Engineering, Zhejiang University, Hangzhou 310027, China (e-mail: hong_li@zju.edu.cn).

Changdong Wang is with the School of Electronic and Information Engineering, Harbin Institute of Technology, Harbin 150001, China (e-mail: hitwcd@stu.hit.edu.cn).

Yongqi Chang is with the Department of Control Science and Engineering, Harbin Institute of Technology, Harbin 150001, China (e-mail: 21b304006@stu.hit.edu.cn).

Color versions of one or more figures in this article are available at https://doi.org/10.1109/TPEL.2024.3454152.

Digital Object Identifier 10.1109/TPEL.2024.3454152

I. Introduction

POWER electronics technologies play a crucial role in contemporary and prospective industrial applications [1], [2], [3], facilitating efficient power conversions that drive advancements toward Industry 4.0 [4] and sustainable energy [5]. The reliability and safety of power electronics devices are of paramount importance in the initial design stage, significantly affecting their operational stability, efficiency, and lifespan [6], [7], [8]. The advent of wide-bandgap semiconductors and fast switching has resulted in high *dv/dt* and *di/dt* in power electronics devices, leading to significant conducted electromagnetic interference (EMI) emissions [9], [10], [11]. Owing to the necessity of electromagnetic compatibility (EMC) to ensure the reliability and safety of power electronics devices, there has been a significant surge in research focused on developing effective countermeasures to suppress the conducted EMI emissions [12], [13], [14].

For existing conducted EMI mitigation techniques, Fig. 1 shows a classification diagram based on the relevant principles [15]. Conducted EMI emissions caused by power electronics devices can be reduced at the source by rearranging the circuit and layout to limit noise propagation [16], [17], [18], using advanced control strategies to alter the noise frequency distribution [19], [20], [21], or implementing soft switching transitions to moderate the rapid variations in *dv/dt* and *di/dt* [22], [23], [24]. Although these techniques can diminish EMI and preserve compact product dimensions to some extent, their design complexity and prototype iteration cycles constrain their versatility [15]. In contrast, EMI emissions can also be suppressed along the propagation path [25], such as by installing EMI filters at the input or output of devices, which offers greater flexibility and effectiveness. Specifically, these EMI filters can be divided into three categories based on their component types: passive EMI filters, active EMI filters [26], [27], [28], [29], and hybrid EMI filters [30], [31], [32]. Passive EMI filters, comprising EMI filtering chokes and capacitors [33], provide substantial noise suppression but are often large in volume and weight. Although active EMI filters are smaller in size owing to the utilization of active components such as amplifiers and transistors, their performance is limited, particularly at high frequencies above tens of megahertz [29]. Thus, by combining both passive and

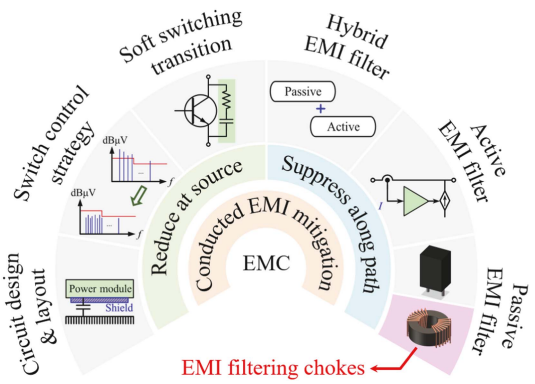

Fig. 1. Classification of existing conducted EMI mitigation techniques used in power electronics.

active components, a hybrid EMI filter can achieve an optimal tradeoff between efficiency and compactness. Currently, employing passive EMI filters remains the prevalent solution in the industry. Since EMI filtering chokes offer considerable noise mitigation and constitute the bulk of the size and mass of an EMI filter, they are attracting widespread focus [34].

To date, various works have been reported on EMI filtering chokes, with significant studies on their characterization and circuit modeling. The first part focuses on quantifying the characteristics of EMI filtering chokes, particularly their frequency-dependent impedance information. The second part involves constructing equivalent circuit models utilizing the characterized information for EMI prediction and performance evaluation in an entire power electronics system. Ultimately, these works aim to optimize the EMI filter design, considering performance, weight, and size [35], [36], [37].

To the best of our knowledge, this article offers the first comprehensive review of EMI filtering chokes, as used in power electronics, with a specific focus on their characterization and circuit modeling. It begins with a brief description of EMI filtering chokes, involving their types, structures, operational principles, critical information, and natural modes. Then, this article delves into the analytical, numerical, and measurement methods for the characterization of EMI filtering chokes, followed by a discussion of their distributed, lumped, and multistage circuit models along with the relevant parameterization methods. Furthermore, existing challenges and ongoing trends are highlighted, and potential research topics are suggested, including characterizing chokes at higher frequencies, assessing choke behaviors in various environments, extending the frequency range and performance of chokes and filters, and incorporating artificial intelligence (AI) in EMI filtering chokes. The main contributions of this article include the following aspects.

1) Investigating existing characterization methods for EMI filtering chokes, including analytical, numerical, and measurement approaches, and discussing their advantages and disadvantages in terms of implementation complexity, accuracy, applicable range, etc.
2) Analyzing and comparing distributed, lumped, and multistage circuit models for EMI filtering chokes. Based on the parameterization methods, case studies, frequency range, accuracy, and physical relevance, the reported works have been summarized as a guideline.
3) Discussing and recommending some prospective topics on suppressing the increasing EMI concerns in power electronics applications.

The rest of this article is organized as follows. Section II presents a brief introduction to EMI filtering chokes. Section III studies and compares existing characterization methods for chokes. Section IV discusses how to use the characterized data to realize choke circuit modeling. Section V outlines future trends in this field and highlights several potential research topics. Finally, Section VI concludes the article.

II. Fundamental Knowledge of EMI Filtering Chokes

Before delving into the characterization and circuit modeling of EMI filtering chokes, this section provides fundamental information about them, including types, structures, operating principles, key characteristics, and natural modes.

A. Types and Structures

EMI filtering chokes, also known as EMI filtering inductors, are typically classified into three categories: differential-mode chokes (DMCs), single-phase common-mode chokes (CMCs), and three-phase CMCs [38], [39], [40]. Fig. 2 depicts their typical structures. Each type of choke consists of a magnetic core wrapped with winding coils. Specifically, a DMC features one winding with two terminals A_1 and A_2, while the single-phase CMC contains two windings and four terminals (i.e., A_1, A_2, B_1, and B_2). A three-phase CMC typically comprises three windings with six terminals labeled A_1, A_2, B_1, B_2, C_1, and C_2. The magnetic core is usually made from high-permeability materials spanning a wide frequency range, such as MnZn/NiZn ferrite and nanocrystalline [41], [42], [43]. For their geometrical structures, a toroid-shaped magnetic core is often preferred for industrial products due to its excellent electromagnetic efficiency and compact physical dimensions. In addition, this design enables an even distribution of winding coils around the magnetic cores' entire circumference, aiding in heat dissipation and reducing mode transformation caused by imbalances.

Beyond the toroid-shaped core, alternative shapes such as UU [44], UI [45], EE [46], and EI [47], as shown in Fig. 3, are tailored for specific applications. Their flatter structure accommodates unique windings, such as planar traces in printed circuit boards (PCBs) [48] and flexible multilayer foils [49], for achieving an integrated design. These configurations may suffer from higher magnetic flux leakage, limited current capacity, and poorer heat dissipation, restricting their applicability to certain uses. In this article, the reported characterization and circuit modeling methods will be elaborated and discussed using examples of EMI filtering chokes with toroid-shaped magnetic cores. However, it should be noted that most of these methods are also compatible with and applicable to chokes using other types of magnetic cores depicted in Fig. 3.

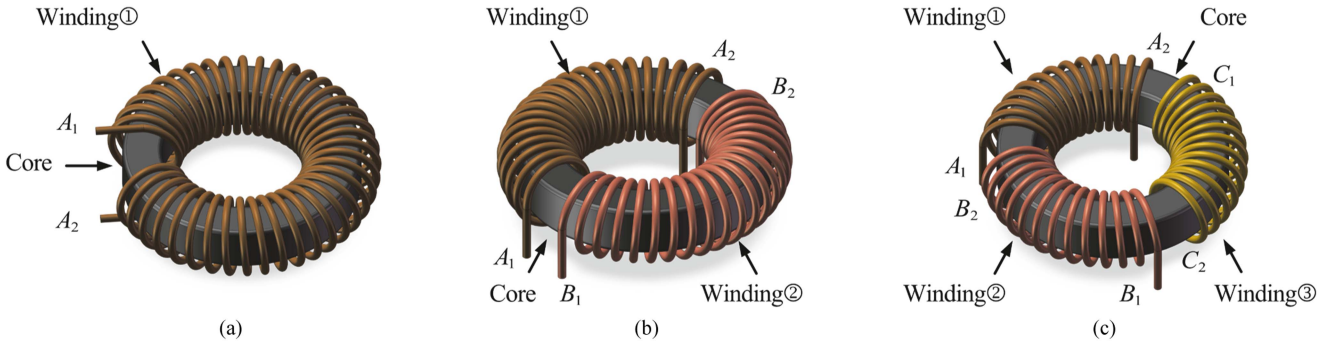

Fig. 2. Typical EMI filtering chokes used in power electronics applications. (a) DMC. (b) Single-phase CMC. (c) Three-phase CMC.

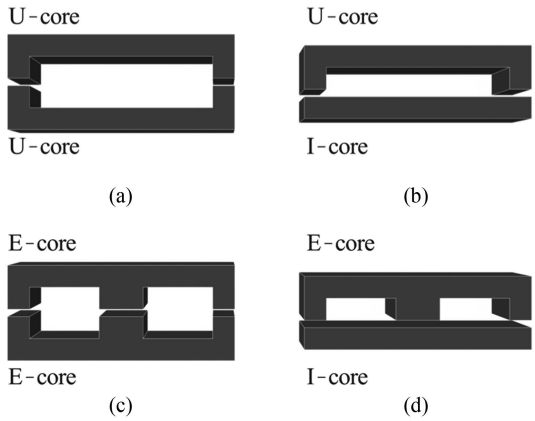

Fig. 3. Structures of other magnetic core types. (a) UU core. (b) UI core. (c) EE core. (d) EI core.

B. Operating Principles

Fig. 4 illustrates the operating principle of EMI filtering chokes in single- and three-phase power electronics systems with a noise source and load [50]. Consisting with Fig. 2, A_1, A_2, B_1, B_2, C_1, and C_2 represent the terminals of EMI filtering chokes, which have three different windings $A1A2$, $B1B2$, and $C1C2$. I_{DM} and I_{CM} represent the respective differential-mode (DM) and common-mode (CM) currents in the power electronics systems, while $I_{\mathrm{DM},i}$ and $I_{\mathrm{CM},i}$ ($i = A$, B, and C) denote the respective DM and CM currents traveling in each winding. Furthermore, ϕ_{DM} and ϕ_{CM} represent the resultant magnetic flux in DM and CM cases, respectively, which are derived from the individual magnetic flux generated by each winding (ϕ_{A1A2}, ϕ_{B1B2}, and ϕ_{C1C2}).

DMCs are utilized in both single- and three-phase systems, positioned on each line to mitigate DM noise [51]. As DM current traverses winding A_1A_2, it generates an enhanced magnetic field, significantly increasing the line impedance to suppress DM emissions. CMCs primarily address CM emissions, which usually appear on two or three power lines and return through the ground [52]. Specifically, a single-phase CMC has two coupled windings and targets single-phase systems. When the CM current enters the single-phase CMC at terminals A_1 and B_1, and exits at terminals A_2 and B_2 [refer to Fig. 4(b)], the magnetic fluxes generated by each winding (i.e., ϕ_{A1A2} and ϕ_{B1B2}) combine, creating CM impedance to impede CM noise. Ideally, in DM scenarios, the DM current travels in the live and neutral lines in opposite directions, and the corresponding flux cancels each other. Nonetheless, due to the inherent leakage inductance of the single-phase CMC, it also exhibits certain DM impedance, aiding in the suppression of DM emissions [53], [54]. Likewise, the three-phase CMC creates considerable CM impedance for CM noise mitigation in a three-phase system by driving a superimposed magnetic field, as shown in Fig. 4(c). However, the DM current flows through its two windings (e.g., A_1A_2 and B_1B_2) and back via the third one (e.g., C_1C_2), resulting in three distinct DM configurations with three distinct DM impedances. Considering achieving perfect structural symmetry for three-phase CMC's windings is challenging due to the industrial manufacturing tolerance, these three DM impedances usually exhibit different frequency response characteristics.

Both DM and CM impedances of EMI filtering chokes vary with frequency, and they cannot be regarded as ideal inductors [55]. For instance, they exhibit resistive behavior at low frequencies due to copper and core losses, while capacitive parasitics such as turn-to-turn and turn-to-core capacitances become significant at high frequencies [56], [57], [58]. According to conducted EMI standards, their impedance characteristics are generally explored at frequencies up to 30 MHz (e.g., CISPR-22 [59]) or even 152 MHz (e.g., DO-160 [60]). In addition, these chokes play potential roles in mitigating radiated EMI emitted from cables in the power electronics systems [61] and enhancing the immunity of critical electronic devices against intentional EMI threats [62].

C. Critical Information

Impedance information is pivotal for gauging the mitigation capabilities of EMI filtering chokes, indicating their efficacy in blocking noise currents across various frequencies [63]. Since most conducted EMI standards primarily concentrate on DM and CM noise levels [64], both DM and CM impedances of EMI filtering chokes are of great importance for system analysis and filtering optimization [65]. Fig. 5(a)–(c) shows the definitions of DM and CM impedances (Z_{DM} and Z_{CM}) for

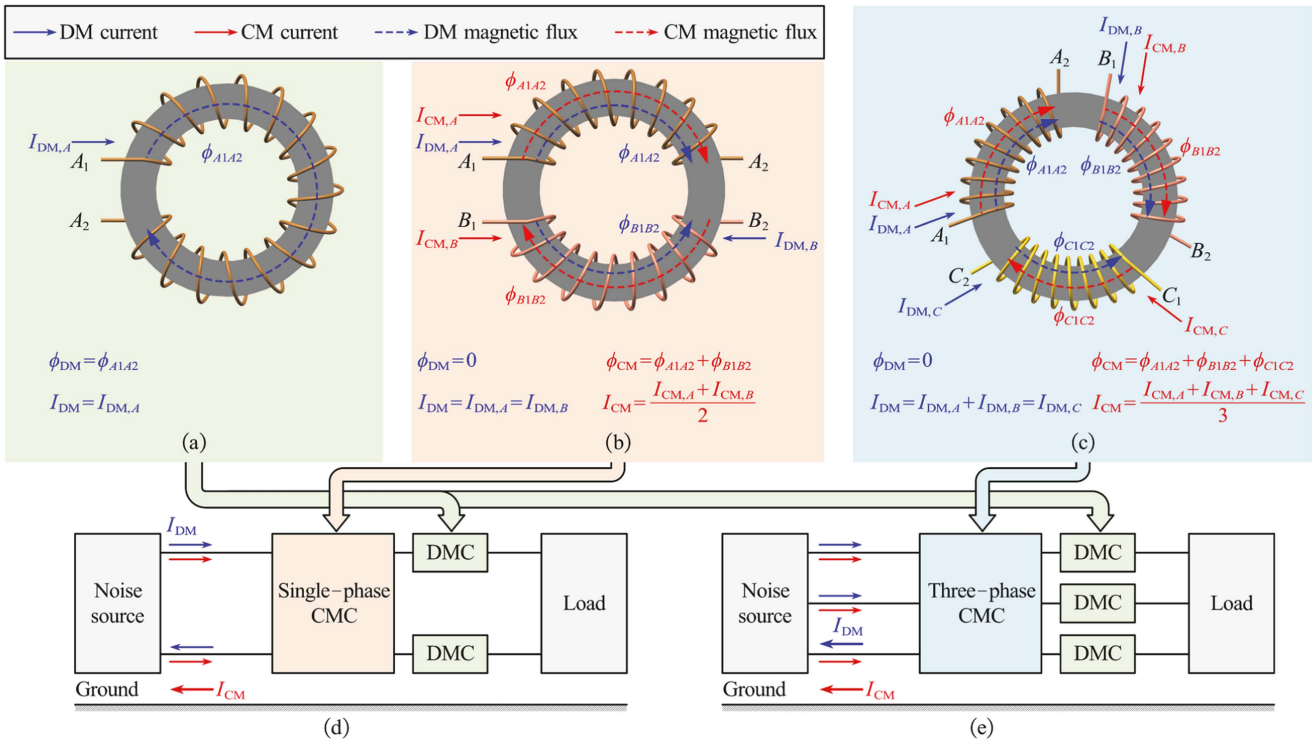

Fig. 4. Operating principles of EMI filtering chokes. (a) DMC. (b) Single-phase CMC. (c) Three-phase CMC. (d) Single-phase power electronics system. (e) Three-phase power electronics system.

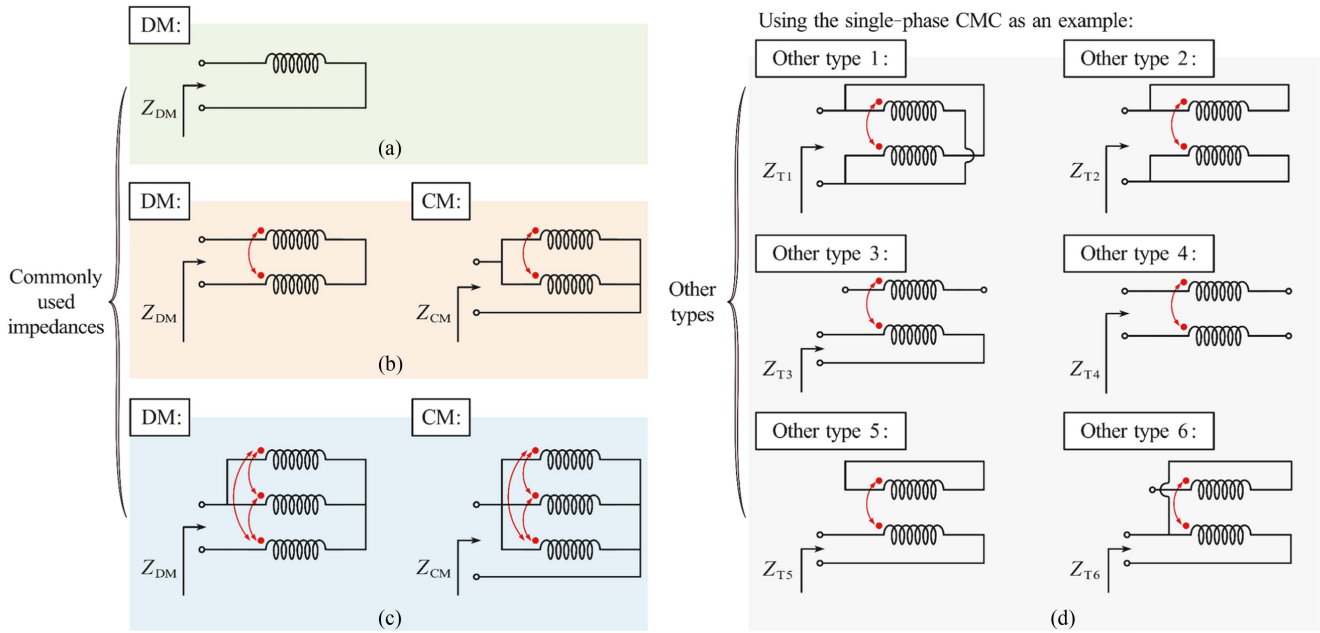

Fig. 5. (a) DM impedance type for DMC. (b) DM and CM impedance types for single-phase CMC. (c) DM and CM impedance types for three-phase CMC. (d) Other impedance types using single-phase CMC as an illustration, where other types 1, 2, 3, 5, and 6 appeared in [67] and other type 4 appeared in [68].

DMCs, single-phase CMCs, and three-phase CMCs, separately [66]. It should be noted that a CMC is actually a network with four, six, or eight ports, while the impedance is by definition a two-terminal concept. Therefore, different impedances can be measured on a CMC depending on the selection of terminals for input and output, as well as the configuration of the remaining terminals. For the sake of brevity, we will refer to these impedances as "impedance types" in this review. These comprehensive data facilitate a more precise equivalent circuit model for systematic EMI simulations [67], [68], [69]. For instance,

Fig. 5(d) showcases various other types using the single-phase CMC as an example, where $Z_{\mathrm{T}j}$ ($j \in \{1, \ldots, 6\}$) denotes the specific impedances for each type.

As an alternative, scattering parameters (*S*-parameters) offer another avenue for evaluating the mitigation effectiveness of EMI filtering chokes [70]. These *S*-parameters can typically be converted into impedance information using port network concepts [71]. For example, in a one-port configuration, the impedance information (Z) can be derived from the reflection coefficient (S_{11}) as follows [72]:

$$Z = Z_0 \frac{1 + S_{11}}{1 - S_{11}} \tag{1}$$

where Z_0 denotes the normalized impedance of the port, usually equal to 50 Ω when employing a vector network analyzer (VNA) for characterization. The impedance information (Z) can also be calculated through a series-through two-port setup, as detailed in [73]

$$Z = Z_0 \frac{(1 + S_{11})(1 + S_{22}) - S_{21}S_{12}}{2S_{21}} \tag{2}$$

where S_{22} is the reflection coefficient from port 2 of the two-port configuration. Both S_{21} and S_{12} represent the transmission coefficients. Moreover, the magnitude of S_{21} can be used to quantify the suppression level of a signal passing through the component by computing the insertion loss (IL), which is given by

$$\mathrm{IL}\ (\mathrm{dB}) = -20\log_{10}(|S_{21}|). \tag{3}$$

Both impedance information and *S*-parameters data provide valuable perspectives for performance assessments of EMI filtering chokes, with selection contingent upon specific user conditions, demands, and objectives.

D. Natural Modes

As mentioned, EMI filtering chokes are primarily used to suppress DM and CM noises propagating in the power line [74]. To express the responses of CMCs in any measurement setup in terms of their reactions to canonical excitations, natural modes provide more insights, which greatly facilitates correlating various impedance types with CMCs' characteristics to CM and DM noises [75], [76]. As a result, performing the modal analysis on EMI filtering chokes simplifies the interpretation of measurement results and aids in the development of a comprehensive circuit model. For recommendations, Ojeda-Rodríguez et al. [75], [76] have explored and detailed the modal theory for various types of CMCs, serving as good benchmarks on the subject.

Building on the fundamental knowledge introduced in this part, the subsequent sections will review and compare existing characterization and circuit modeling methods for EMI filtering chokes used in power electronics. These efforts aim to aid in component selection, EMI performance evaluation, and system simulation, ultimately achieving optimal EMI filter design without a trial-and-error process.

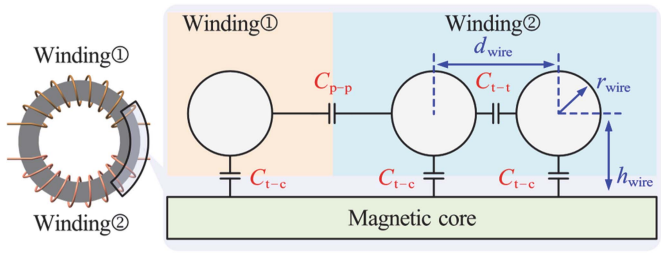

Fig. 6. Parasitic capacitances in a single-phase CMC with bare windings.

III. Characterization of EMI Filtering Chokes

To achieve impedance or *S*-parameters characterization of EMI filtering chokes, various studies have been reported, which can essentially be divided into three categories based on the implemented principles, namely analytical, numerical, and measurement methods.

A. Analytical Methods

Analytical methods typically characterize the impedance data of EMI filtering chokes using mathematical formulations and equations based on the principles of electromagnetism and circuit theory. These methods often involve simplifications and assumptions to create solvable functions. Generally, to derive the impedance frequency responses of EMI filtering chokes, there are six important parameters: turn-to-turn capacitance $C_{\mathrm{t-t}}$, turn-to-core capacitance $C_{\mathrm{t-c}}$, core loss R_{core}, winding resistance R_{wire}, self-inductance L_{self}, and leakage inductance L_{leak} [77]. Their corresponding definitions and derivations are introduced as follows.

For capacitances, $C_{\mathrm{t-t}}$ represents the parasitic capacitance between adjacent turns of a winding, while $C_{\mathrm{t-c}}$ denotes the capacitance between each turn and the magnetic core, as depicted in Fig. 6. Moreover, when two windings of a single-phase are close together, the stray capacitance between these two-phase windings $C_{\mathrm{p-p}}$ can be calculated in a similar way to $C_{\mathrm{t-t}}$. In general, the line charge approximation concept is adopted to simplify the computation of these capacitances [78]. In [79], the per unit length (PUL) values of $C_{\mathrm{t-t}}$ and $C_{\mathrm{t-c}}$ can be calculated by

$$C_{\mathrm{t-t}}\ (\mathrm{PUL}) = \frac{\pi\varepsilon_0}{\ln\left[\frac{d_{\mathrm{wire}}}{2r_{\mathrm{wire}}} + \sqrt{\left(\frac{d_{\mathrm{wire}}}{2r_{\mathrm{wire}}}\right)^2 - 1}\right]}$$

$$C_{\mathrm{t-c}}\ (\mathrm{PUL}) = \frac{2\pi\varepsilon_0}{\ln\left[\frac{d_{\mathrm{wire}}}{2r_{\mathrm{wire}}} + \sqrt{\left(\frac{d_{\mathrm{wire}}}{2r_{\mathrm{wire}}}\right)^2 - 1}\right]} \tag{4}$$

where ε_0 is the permittivity of air, and other parameters are defined in Fig. 6 [80]. However, the equations in (4) only consider bare winding coils, which might not be practical for a real choke. To account for the influences of insulation layers, another capacitance configuration, as shown in Fig. 7(a), was developed in [81] and [82]. The calculations were simplified by assuming close alignment of turn-to-core and turn-to-turn to

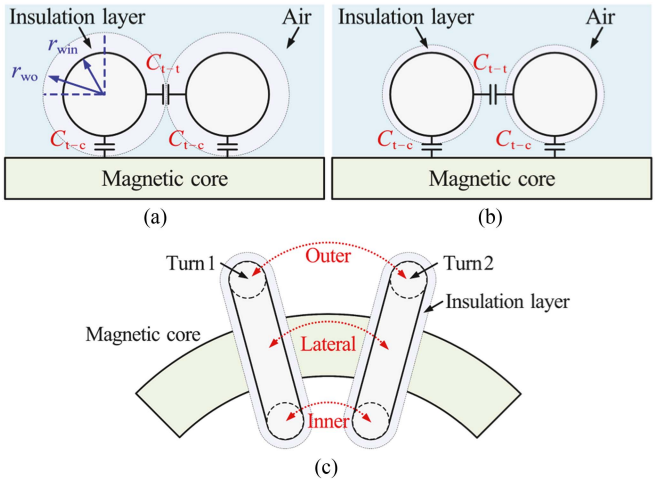

Fig. 7. Schematic diagrams of capacitance configurations. (a) With insulation layer and closely distributed. (b) With insulation layer and air gap. (c) With sparsely wound windings.

estimate the air gap capacitance. The corresponding PUL values of capacitances $C_{\mathrm{t-t}}$ and $C_{\mathrm{t-c}}$ are determined by [82]

$$C_{\mathrm{t-t}}\ \text{(PUL)} = \frac{2\varepsilon_0}{\sqrt{\left[1+\frac{1}{\varepsilon_r}\ln\left(\frac{r_{\mathrm{wo}}}{r_{\mathrm{win}}}\right)\right]^2-1}}\tan^{-1}\left[\sqrt{\frac{2+\frac{1}{\varepsilon_r}\ln\left(\frac{r_{\mathrm{wo}}}{r_{\mathrm{win}}}\right)}{\frac{1}{\varepsilon_r}\ln\left(\frac{r_{\mathrm{wo}}}{r_{\mathrm{win}}}\right)}}\right]$$

$$C_{\mathrm{t-c}}\ \text{(PUL)} = \frac{4\varepsilon_0}{\sqrt{\left[1+\frac{1}{\varepsilon_r}\ln\left(\frac{r_{\mathrm{wo}}}{r_{\mathrm{win}}}\right)\right]^2-1}}\tan^{-1}\left[\sqrt{\frac{2+\frac{1}{\varepsilon_r}\ln\left(\frac{r_{\mathrm{wo}}}{r_{\mathrm{win}}}\right)}{\frac{1}{\varepsilon_r}\ln\left(\frac{r_{\mathrm{wo}}}{r_{\mathrm{win}}}\right)}}\right]. \quad (5)$$

In (5), ε_r represents the relative permittivity of the insulation layer. As shown in Fig. 7(a), r_{win} and r_{wo} denote the inner and outer radius of the insulation layer, respectively. Due to the inherent hardness and elastic modulus of the copper material in the windings, air gaps between turns and the core are often inevitable in industrial manufacturing. Therefore, an enhanced configuration was developed in [83], with a relevant schematic diagram depicted in Fig. 7(b). Furthermore, the variation of d_{wire} from the core's inner to outer diameter has been taken into account, making it applicable to EMI filtering chokes with sparsely wound windings, as illustrated in Fig. 7(c) [83]. In this context, $C_{\mathrm{t-t}}$ and $C_{\mathrm{t-c}}$ can be approximated as

$$\begin{aligned} C_{\mathrm{t-t}} &= C_{\mathrm{t-t,in}} + C_{\mathrm{t-t,o}} + 2C_{\mathrm{t-t,l}} \\ C_{\mathrm{t-c}} &= C_{\mathrm{t-c,in}} + C_{\mathrm{t-c,o}} + 2C_{\mathrm{t-c,l}} \end{aligned} \quad (6)$$

where $C_{\mathrm{t-t,in}}$, $C_{\mathrm{t-t,o}}$, and $C_{\mathrm{t-t,l}}$ represent the inner, outer, and lateral parts of the turn-to-turn capacitance $C_{\mathrm{t-t}}$, respectively. Similarly, $C_{\mathrm{t-c,in}}$, $C_{\mathrm{t-c,o}}$, and $C_{\mathrm{t-c,l}}$ denote the components of the turn-to-core capacitance $C_{\mathrm{t-c}}$. The derivation of these capacitances involves complex integral calculations, which have been detailed in [83].

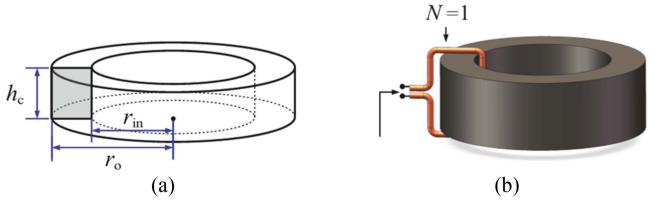

Fig. 8. (a) Geometrical structure of a magnetic core. (b) Measurement setup for determining μ, μ', and μ''.

In addition to the derivations of $C_{\mathrm{t-t}}$, $C_{\mathrm{t-c}}$, and $C_{\mathrm{p-p}}$, some investigations have also reported the influence of ferrite and nanocrystalline materials [84], where the introduced core capacitance was derived as detailed in [85]. Alternatively, electric field energy analysis can also assist in the calculation of parasitic capacitances [86], [87]. These works provide more precise values at the cost of increased complexity. The aforesaid literature primarily targets capacitance calculations to aid in the prediction of resonant frequencies. To obtain a complete impedance frequency response, they may necessitate the assistance of other methods [83], such as measurements [82], to gather inductance and resistance data. Therefore, these methods are regarded as semi-analytical.

For full analytical methods, they can furnish extensive impedance information of EMI filtering chokes in the absence of a real product. This helps optimize the material selection, winding strategy, and core dimensions in the initial design stage. Muetze [88] directly determined L_{self} by employing the toroidal inductance formula, whereas Massarini et al. [89] derived this value by solving a complex matrix that includes both self and mutual inductances of all individual turns. Since they overlooked the frequency-dependent permeability of the magnetic core, the derived L_{self} was applicable only at a single frequency point. By applying the frequency-dependent permeability μ, L_{self} in the frequency range of interest can be calculated as follows [90]:

$$L_{\mathrm{self}} = \frac{\mu' h_{\mathrm{c}} N^2}{2\pi \ln\left(\frac{r_{\mathrm{in}}}{r_{\mathrm{o}}}\right)} \quad (7)$$

$$\mu = \sqrt{(\mu')^2 + (\mu'')^2} \quad (8)$$

where h_{c}, r_{in}, and r_{o} represent the height, inner radius, and outer radius of the core, respectively, as shown in Fig. 8(a). N is the number of turns in each winding. In addition, μ' and μ'' are the real and imaginary parts of μ, respectively, which can be obtained from a datasheet or via a one-turn measurement, as established in Fig. 8(b) [91]. Similar derivations have been employed in [77], [92], and [93], allowing for the estimation of the DM inductance of a DMC and the CM inductance of a CMC. To improve accuracy, L_{leak} is suggested to be calculated, which can also be used to determine the DM inductances of CMCs. In [54], the toroid core of an EMI filtering choke is reshaped into a rod structure to compute L_{leak}. Based on the empirical formulas reported in [54], a new empirical expression

for L_{leak} was developed in [77] to directly derive an effective mean path length of the toroid core. The resultant equations for computing L_{leak} of both single- and three-phase CMCs have been summarized in [92], given by

$$L_{\text{leak}} \cong 2.5\mu_0 N^2 \frac{h_{\text{c}}\left(r_{\text{o}}-r_{\text{in}}\right)}{l_{\text{eff}}}\left[\frac{l_{\text{e}}}{2}\sqrt{\frac{\pi}{h_{\text{c}}\left(r_{\text{o}}-r_{\text{in}}\right)}}\right]^{1.45} \tag{9}$$

where μ_0 is the vacuum permeability and l_{e} denotes the mean path length of the toroid core. For the single-phase CMC, the effective mean path length l_{eff} can be derived as [54]

$$l_{\text{eff}} \cong l_{\text{e}}\sqrt{\frac{\theta}{2\pi}+\frac{1}{\pi}\sin\left(\frac{\theta}{2}\right)} \tag{10}$$

where θ is the circular angle occupied by each winding [92]. For the three-phase CMC, the related l_{eff} is given by [77]

$$l_{\text{eff}} \cong 2\sqrt{\frac{{r_{\text{o}}}^2}{\sqrt{2}}\left[\frac{\theta}{4}+1+\sin\left(\frac{\theta}{2}\right)\right]^2+{r_{\text{in}}}^2\left[\frac{\theta}{4}-1+\sin\left(\frac{\theta}{2}\right)\right]^2}. \tag{11}$$

In addition to using these empirical formulas, the leakage inductance of each turn can be calculated through field analysis [94]. This approach is beneficial for developing a distributed circuit model of an EMI filtering choke, facilitating the analysis of each turn to optimize the winding distribution. However, its complexity increases with the number of turns.

Besides inductances and capacitances, resistive parameters also play a significant role in defining the impedance frequency responses of EMI filtering chokes. For the small signal model, Kovacic et al. [94] derived R_{core} using imaginary parts of core permeability directly, as given by

$$R_{\text{core}} = \frac{\mu'' h_{\text{c}} N^2}{2\pi \ln\left(\frac{r_{\text{in}}}{r_{\text{o}}}\right)}. \tag{12}$$

However, for scenarios with large signals, both hysteresis and residual losses should be taken into account [95]. Using Steinmetz's coefficients, Heldwein et al. [77] provided a correction formula, while Han et al. [93] estimated the core loss by utilizing the flux density frequency response as an alternative. Following [77], the large signal core losses R_{core} can be modeled as

$$R_{\text{core}} = 2V_{\text{c}}K_{\text{c}}f^{\alpha}I_{\text{rms}}^{\beta-2}\left(\frac{A_{\text{L}}N\mu'}{A_{\text{e}}\left|\mu\left(f = 0\text{ Hz}\right)\right|}\right)^{\beta} \tag{13}$$

where V_{c} represents the volume of the core; K_{c}, α, and β are the Steinmetz loss coefficients; I_{rms} denotes the root-mean-square current; A_{L} is the inductance per turn for the given core; A_{e} denotes the core effective area. Typically, employing (12) to design an EMI filtering choke is sufficient unless it will be installed in a high-current application. As for R_{wire}, it is usually dominant in the low-frequency range (i.e., <10 kHz), making it necessary to build a wideband circuit model of the choke. It includes the dc resistance ($R_{\text{wire,dc}}$) due to material properties and the ac resistance ($R_{\text{wire,ac}}$) due to the skin and proximity effects, which are expressed by [77]

$$R_{\text{wire,dc}} = \frac{l_{\text{w}}\rho_{\text{w}}}{\pi r_{\text{wire}}} \tag{14}$$

$$R_{\text{wire,ac}} \cong R_{\text{wire,dc}}\cdot\left(\frac{\pi}{4}\right)^{\frac{3}{4}} \cdot\frac{\sqrt{\left(2r_{\text{wire}}\right)^3}}{\delta\sqrt{d_{\text{wire}}}}\cdot\left[1+\frac{2\left({N_{\text{layer}}}^2-1\right)}{3}\right] \tag{15}$$

where l_{w} is the length of the wire; ρ_{w} defines its resistivity; δ represents the skin depth; N_{layer} denotes the number of layers in each winding. The derivation details of R_{wire} can be found in [77], [92], and [93].

Beyond deriving *RLC* parameters, applying transmission line theory may also be effective in characterizing the choke [96]. While its utility may extend to 1 GHz, Mu et al. [96] only verified this capability using a choke with a one-turn structure.

Table I tabulates and compares the analytical methods for impedance characterization of chokes, including their identified parameters, case studies, and demonstrated data. It should be noted that the frequency range and accuracy of the analytical methods listed in Table I are based on their respective experimental or simulation results. To evaluate the accuracy level, a classification criterion is employed, given by

$$\text{Accuracy}\begin{cases}\text{Low}, & \text{if } Error_{\text{Max}} > 6\text{ dB}\\ \text{Moderate}, & \text{if } 3\text{ dB} < Error_{\text{Max}} \le 6\text{ dB}\\ \text{High}, & \text{if } Error_{\text{Max}} \le 3\text{ dB}.\end{cases} \tag{16}$$

In (16), the maximum impedance magnitude error $Error_{\text{Max}}$ at each frequency serves as the index for accuracy, aligning with worst-case considerations in EMC design. Typically, the industry standard for EMI filtering design includes a 6 dB margin [35]; thus, the accuracy is defined as "Low" when $Error_{\text{Max}} > 6$ dB. Moreover, to further distinguish between accuracy levels, 3 dB is applied as the boundary, "Moderate" accuracy for 3 dB $< Error_{\text{Max}} \le 6$ dB, and "High" accuracy for $Error_{\text{Max}} \le 3$ dB. Besides, it should be noted that some studies solely employ analytical calculations for choke design without involving formula validations, while some others may only verify specific parameters (e.g., $C_{\text{t-t}}$) without determining the resultant DM and CM impedances.

B. Numerical Methods

Numerical methods extract impedance frequency responses of EMI filtering chokes typically by solving intricate three-dimensional (3-D) models using electromagnetic software and computational techniques. Prominently used techniques include the finite element method (FEM), finite-difference time-domain (FDTD), partial element equivalent circuit (PEEC), and PEEC with boundary integral method (PEEC-BIM). Table II tabulates some merits and disadvantages of these methods.

FEM applies Maxwell's equations by breaking the entire computational area into a finite set of small elements. This method is effective for impedance characterization of EMI filtering chokes,

TABLE I
COMPARISON OF SEMIANALYTICAL AND FULLY ANALYTICAL METHODS FOR IMPEDANCE EXTRACTION OF EMI FILTERING CHOKES

Ref.	Method	Identified parameters							Case studies			Demonstrated information				
		L_{self}	L_{leak}	R_{core}	R_{wire}	C_{t-t}	C_{t-c}	C_{p-p}	Choke type	Winding layer number	No. of turns per phase	Frequency range (Hz)	Accuracy	Value		Mode	
														Mag	Pha	CM	DM
[79]	Semi-analytical	Need to combine with other methods to obtain key values, such as inductance				√	√		○	Single	25	20 k – 30 M	Low	√			√
[81]						√	√		N/P	Single/Multiple	95	N/P	High				
[82]						√	√		○	Single	17	1 k – 100 M	Moderate	√			√
[83]						√	√	√	◎	Single	16	10 k – 50 M	High	√		√	√
[84]						√	√		◎●	Single	1–40	10 k – 50 M	High	√		√	√
[85]						√	√		○	Single	4/6/15/34	150 k – 30 M	Moderate	√			√
[86]						√	√		○	Single	6–24	N/P	Moderate	√	√		√
[77]	Full-analytical	√	√	√	√	√	√		●	Single	8/10	100 – 100 M	Low	√		√	
[89]		√				√	√		N/P	Single/Multiple	38/47/50/80	N/P	High				
[92]		√	√	√	√	√			◎●	Single	18/40	10 k – 30 M	Low	√	√	√	
[93]		√	√	√	√	√			●	Single	N/P	10 k – 50 M	N/P	√		√	
[94]		√	√	√		√	√		◎●	Single	5/9	1 k – 100 M	Low	√			
[96]									○	Single	1	10 k – 1 G	Moderate	√	√		√

*Acronyms and symbols:
○ Differential-mode choke
◎ Single-phase common-mode choke
● Three-phase common-mode choke
N/P Not provided
Mag Magnitude
Pha Phase
CM Common-mode
DM Differential-mode

TABLE II
INTRODUCTION OF TYPICAL NUMERICAL SIMULATION METHODS

Methods	Merits and demerits
FEM	☑ It is suitable to handle complex geometries and boundary conditions and can analyze field distribution in details. ☒ It requires high computation resources.
FDTD	☑ It provides intuitive time-domain results and is suitable for analyzing wideband and nonlinear materials. ☒ Its simulation accuracy is limited for items with complex structures.
PEEC	☑ It offers RLC parameters directly with fast computation speed, facilitating integration with circuit simulation. ☒ It is less accuracy than solving the Maxwell equations, especially for core with nonlinear permeability.
PEEC-BIM	☑ It combines the advantages of PEEC and BIM, and it is suitable for analyzing the open boundary problems. ☒ Its implementation complexity is relatively high.

allowing for their 3-D modeling with discrete winding turns, as depicted in Fig. 9. Such a setup enables the analysis and parameters extraction of each turn, such as C_{t-t}, making it beneficial for choke optimization. However, it requires creating the excitation for each turn, thereby complicating the setting process in numerical simulation. While this strategy has been used to extract the *RLC* matrices of each turn and assess the performance of a three-phase CMC [97], the accuracy is constrained due to the oversight of the frequency-dependent permeability. To account for permeability variations, Fan et al. [35] and Kovačić et al. [66] acquired a series of *RLC* matrices by iteratively adjusting the permeability value at each frequency to derive the impedance frequency response. However, this solution is rather

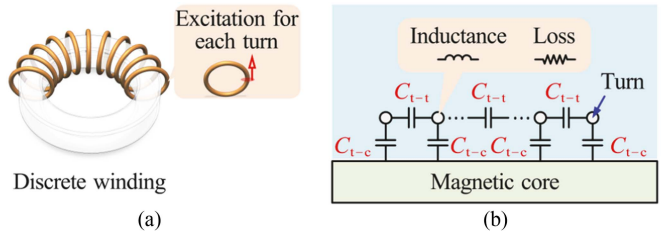

Fig. 9. 3-D model with discrete winding turns. (a) Schematic diagram. (b) Equivalent capacitive network.

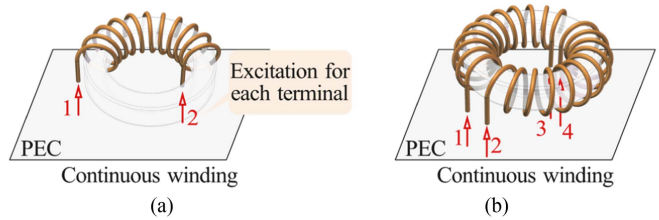

Fig. 10. 3-D model with continuous winding. (a) DMC. (b) Single-phase CMC.

time-consuming. To expedite the process through frequency sweep, a two-dimensional (2-D) solver could be incorporated to extract *RL* parameters; however, the simplification in the 2-D model leads to reduced accuracy at high frequencies [98].

In addition, the 3-D models of winding coils can also be constructed as a continuous configuration, as shown in Fig. 10. This configuration enables the direct inclusion of permeability frequency response, facilitating the acquisition of *S*-parameters.

Similar to Fig. 10(b), a single-phase CMC was modeled with four excitation ports in CST Microwave Studio, where each port acted as the interconnection between the choke terminal and the perfect electric conductor (PEC) ground [99]. While efficient in determining S_{21} of an individual winding, it fell short in acquiring the CM and DM information of a choke with two windings. To derive the CM and DM impedances, the 4×4 *S*-parameters obtained from the setup shown in Fig. 10(b) were decoupled using the mixed-mode theory [100], [101]. However, it may not be applicable for simulating three-phase CMCs with six terminals. To address this issue, Jie et al. [102] analyzed the mixed-mode conversion in three-phase CMC, expanding the scope of this theory. As an alternative, He et al. [103] used additional wires to connect the choke terminals, allowing the behavior of a single-phase CMC to be directly characterized with simulated S_{21} via a two-port series-through setup. This approach avoids the extra processing required by the mixed-mode theory, as reported in [100] and [102]. In addition, to reduce the mesh count and computation resources, the windings were built with square cross sections instead of round cross sections. Following [103], the impact of additional wires was considered, and simulation accuracy can be improved by eliminating these impacts [104].

Some other works employed the FEM to estimate specific parameters rather than the entire impedances. For example, Dong et al. [105] modeled the leakage inductance of CMC chokes through FEM and determined the optimal design via an artificial neural network. A study targeting stray capacitance extraction was conducted in [106], requiring consideration of the series–parallel relationship between $C_{\mathrm{t-t}}$ and $C_{\mathrm{t-c}}$. To simplify the derivations, an improved matrix operation method was proposed to treat the core as an independent node and regard the network as a "black box" [107]. In addition, Salomez et al. [108] and [109] enhanced the winding model to extract accurate parasitic capacitance by taking into account the uneven distribution of the distance between winding turns and the magnetic core.

FDTD acquires the time-domain solution with a single simulation and employs Fourier transformation to determine the relevant frequency responses [110]. It exhibited commendable performance when characterizing a single-turn CMC to assess cable crosstalk [111]. However, for EMI filtering chokes with multiturn windings, the accuracy of FDTD is limited due to its unique Yee lattice or cube mesh.

PEEC converts the electromagnetic analysis into solving the *RLC* parameters and sources within an equivalent network, allowing it to be directly integrated into the systematic circuit simulations [112]. Leveraging PEEC, Eremyan et al. [113] introduced a micromodel for single-phase CMCs to determine their broad-spectrum DM and CM impedances, building the windings with continuous turns. Given that PEEC usually has limitations in handling the nonlinear magnetic materials and the complex geometries, it tends to be less precise than FEM.

PEEC-BIM is a composite solution method that uses PEEC for rapid simulation and incorporates BIM to analyze nonlinear magnetic cores. This method results in higher implementation complexity compared to others. The PEEC-BIM method was first employed for characterizing EMI filtering chokes in [114]. However, the simulation results show significant discrepancies from measurement outcomes above 10 MHz due to insufficient consideration of core permeability and permittivity. Based on [114], both surface current and charge densities of the magnetic core had minimal influence on the impedance characterization of EMI filtering chokes, and therefore, Kovačević et al. [115] reduced these parameters to simply the simulation. By adding more capacitive matrices to account for the core permittivity and $C_{\mathrm{t-c}}$, the simulation accuracy was improved [116]. In addition, PEEC-BIM can encompass all filtering components in a single round, supporting a full simulation of the EMI filter with outcomes of impedances and *S*-parameters data [117]. Similar to PEEC simulations, all windings of EMI filtering chokes must be constructed with continuous turns for PEEC-BIM methods, which means that it is a challenge to analyze the parasitic parameters for each adjacent turn.

Table III compares these numerical works regarding their simulation methods, platforms, complexity, case studies, and validated information. It should be noted that the evaluation of frequency range and accuracy adheres to the same criteria as stated in Table I. Specifically, the frequency range for each work is directly collected from their respective validation results, and the accuracy is classified according to (16). Overall, FEM is the most common method owing to its well-developed commercial software, extensive teaching resources, and wide applicability. Both PEEC and PEEC-BIM methods demonstrate superiorities in network analysis and circuit simulation. Their mesh subdivision often demands substantial computational resources, making the actual simulation speed highly dependent on the capabilities of the workstation used. In addition to the inherent features of each method, the simulation accuracy is significantly affected by the detailed geometric and material properties of EMI filtering chokes. The sensitivities of several critical parameters in choke numerical characterization have been thoroughly investigated, with [100] targeting impedance magnitude and [101] studying phase information.

C. Measurement Methods

Measurement methods characterize EMI filtering chokes by employing high-precision instruments, such as the impedance analyzer (IA) or the VNA [72]. In addition, to be compatible with the nonstandard terminals of EMI filtering chokes (refer to Fig. 2), a fixture adapter is needed to interconnect the IA/VNA and the choke.

Usually, Kelvin clip leads, as demonstrated in Fig. 11(a), are used for measuring components due to their good adaptability to various terminal configurations [118]. However, the effective measurement frequency range of Kelvin clip leads is typically limited to below 1 MHz, rendering them insufficient for characterizing EMI filtering chokes for EMC applications. Another commercial device that supports wideband impedance measurements of leaded components is the Keysight 16047E fixture adapter, as shown in Fig. 11(b) [119]. Due to restrictions regarding the aperture, layout, and number of the component's terminals, this fixture adapter is not suitable for CMCs.

TABLE III
COMPARISON OF NUMERICAL METHODS FOR IMPEDANCE/S-PARAMETERS EXTRACTION OF EMI FILTERING CHOKES

Ref.	Method	Simulation platform	Simulation complexity	Case studies			Demonstrated information					
				Choke type	Winding layer number	No. of turns per phase	Frequency range (Hz)	Accuracy	Value		Mode	
									Mag	Pha	CM	DM
[66]	FEM	Infolytica MagNet	High	⊜●	Single	6/9	1 k – 100 M	Low	√		√	√
[35]		Ansys Maxwell	High	●	Single	10	10 k – 30 M	High	√	√	√	
[97]		Ansys Maxwell	Low	●	Single	5	1 k – 100 M	Low	√		√	√
[98]		Ansys Maxwell	Moderate	⊜	Single	6	10 k – 30 M	Low	√	√	√	
[99]		CST Microwave Studio	Moderate	⊜	Single	30	10 k – 50 M	Moderate	√			
[100]		CST Microwave Studio	Moderate	⊜	Single	5–10	100 k – 1 G	Low	√		√	√
[101]		CST Microwave Studio	Moderate	⊜	Single	5/7/9	10 k – 100 M	High	√	√	√	√
[102]		CST Microwave Studio	Moderate	⊜●	Single	9/11	100 – 120 M	Moderate	√	√	√	√
[103]		CST Microwave Studio	Moderate	⊜	Single	11	100 k – 1 G	Low	√			
[104]		CST Microwave Studio	High	⊜	Single	7	10 k – 100 M	High	√	√	√	√
[111]	FDTD	SEMBA-FDTD	Moderate	○	Single	1	10 M – 1 G	Low	√			√
[113]	PEEC	EMCoS Studio	Moderate	⊜	Multiple	15/40/41	50 – 100 M	Moderate	√		√	√
[114]	PEEC-BIM	N/P	High	○	Single	3/20	1 k – 100 M	Low	√			√
[115]		GeckoEMC	High	○⊜	Single	7/12	10 k – 30 M	High	√		√	√
[116]		GeckoEMC	High	○⊜	Single	20–42	10 k – 30 M	High	√		√	√

*Acronyms and symbols:
○ Differential-mode choke
⊜ Single-phase common-mode choke
● Three-phase common-mode choke
N/P Not provided
Mag Magnitude
Pha Phase
CM Common-mode
DM Differential-mode
FEM Finite element method
BIM Boundary integral method
FDTD Finite-difference time-domain method
PEEC Partial element equivalent circuit

Fig. 11. Commercially available fixture adapters. (a) R&S LCX-Z2 Kelvin clip leads [118]. (b) Keysight 16047E fixture adapter [119].

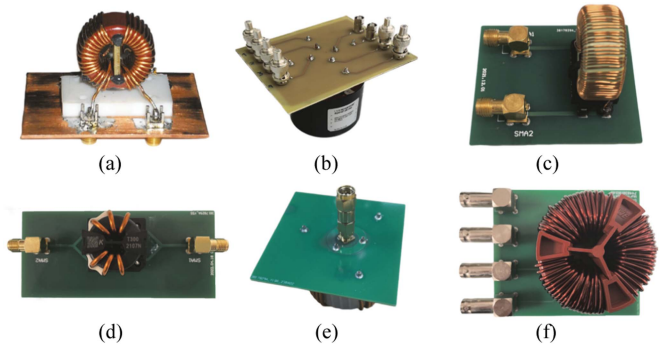

Fig. 12. Prototypes of customized fixture adapters for characterizing the EMI filtering chokes. (a) [121]. (b) [76]. (c) [125]. (d) [127]. (e) [128]. (f) [128].

Given the constraints of existing commercially available fixture adapters, some customized designs have been developed for specific EMI filtering chokes. Targeting single-phase CMCs, Roc'h et al. [120], [121] introduced a four-port fixture adapter to measure the choke impedances using the IA. In this design, each choke terminal was directly connected to the center pin of Subminiature Version A (SMA) connectors, as depicted in Fig. 12(a). Adopting a similar layout, Hu et al. [122] employed fixture adapters to connect the single-phase CMC to a four-port VNA. Relying on mixed-mode theory, both CM and DM impedances of chokes can be calculated from the measured *S*-parameters [123]. For the three-phase CMC with six terminals, a corresponding fixture adapter was developed [76], with its diagram illustrated in Fig. 12(b). These fixture adapters ensure the electrical connectivity of the choke and VNA but introduce unwanted parasitics. Although applying the electrically short concept in these fixture designs can mitigate the parasitics, their effects can still become apparent as the frequency increases, especially at high frequencies [124]. The absence of accuracy verification in [76], [120], [121], [122], and [123] reduces their reliability in choke characterization at high frequencies [124], [125].

To account for the parasitics induced by the fixture adapters and ensure measurement accuracy, several techniques have been developed. A unique two-port fixture adapter was custom-designed for DMC [124]. By treating both signal and return paths as the 50 Ω transmission lines, the magnitude data of

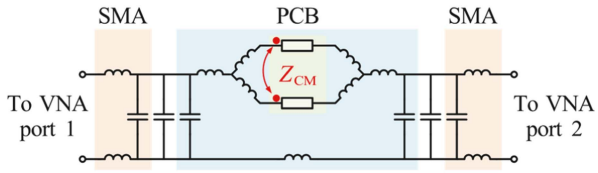

Fig. 13. Equivalent circuit of Fig. 12(d) for CM impedance measurement of a single-phase CMC using the TCD method. Definitions of parameters are detailed in [127].

DMC impedance was inferred by measuring the modulus of S_{21}. However, it was challenging to obtain the accurate lengths of these transmission lines, making the extraction of phase information inaccessible. As an alternative, it is promising to directly counter the parasitic effects from fixture adapters, which can be effectively achieved through de-embedding [125], [126], [127], [128] or calibration [128], [129], [130].

To eliminate the parasitics of the fixture adapter shown in Fig. 12(c) [125], a two-port circuit de-embedding (TCD) method was first proposed for impedance measurements of a DMC. It conducted detailed boundary element analysis for SMA connectors and PCB traces to extract their frequency-dependent parasitics. By constructing the lumped circuit and applying the network analysis concept, the parasitic influence of the fixture adapter can be eliminated from the measurement results. This method has been extended to single-phase CMCs, with the fixture adapter's layout revised to that shown in Fig. 12(d) to minimize mutual coupling between the two SMA connectors [126]. For a detailed conclusion and further refinement, Jie et al. [127] elaborated the details of this method for both DMC and single-phase CMCs and streamlined the lumped circuit by disregarding negligible resistive parasitics. Fig. 13 shows the equivalent circuit of Fig. 12(d) for illustration.

Another technique known as the single-port circuit de-embedding (SCD) method was proposed in [128] to accommodate the one-port topology of fixture adapters shown in Fig. 12(e). Fig. 14(a) establishes its equivalent circuit for DM impedance measurement of a three-phase CMC. This method de-embedded the unwanted parasitics of fixture adapters via boundary element analysis and circuit theory. It has good versatility to be used with either IA or VNA. Both TCD and SCD methods were validated to accurately characterize the choke impedance up to 120 MHz [127], [128]. For a higher frequency range, they are anticipated to sustain the accuracy by employing the VNA and deriving impedance information from the measured *S*-parameters.

Through the calibration concept, the parasitics introduced by the fixture adapters can be compensated for during the measurement process. Based on the interface of customized fixture adapters, Jie et al. [129] designed a series of calibration kits to perform the compensation. By characterizing the nonideal behaviors of these kits, the open-short-load (OSL) calibration technique was applied, achieving good measurement accuracy up to 30 MHz. Another method, namely the three-port network calibration (TNC) method, was developed in [128] to compensate for the induced parasitics in a straightforward manner. A

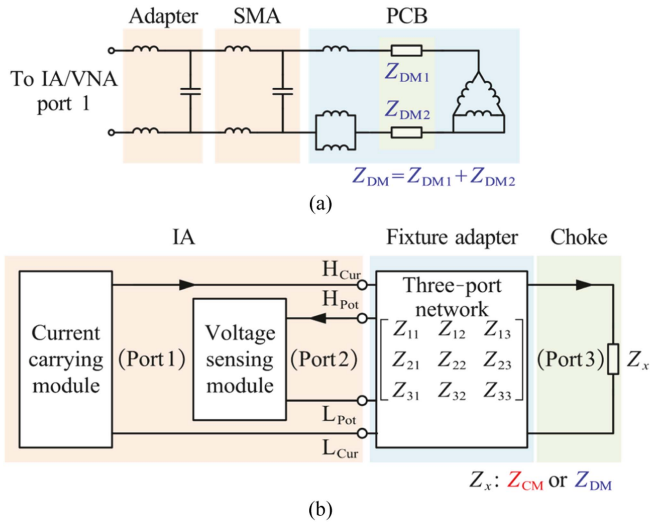

Fig. 14. (a) Equivalent circuit of Fig. 12(e) for DM impedance measurement of a three-phase CMC using the one-port circuit de-embedding method. (b) Schematic diagram of Fig. 12(f) using the TNC for a three-phase CMC. Definitions of parameters are detailed in [128].

series of four-terminal fixture adapters [see Fig. 12(f)] were designed to match the IA interfaces (H_{Cur}, H_{Pot}, L_{Cur}, and L_{Pot} [131], as shown in Fig. 14(b)), and therefore, the schematic diagram of the measurement setup can be built. By dividing the current-carrying and voltage-sensing modules of the IA based on its operational principles, the parasitics and circuits of the fixture adapter can be regarded as a "black box" and represented as a three-port network. Relying on the network analysis concept [132], the actual impedance of the choke (Z_x, x = CM or DM) can be derived by [128]

$$Z_x = \frac{a_1 Z_x^* + a_2}{a_3 Z_x^* - 1} \tag{17}$$

where Z_x^* denotes the uncompensated measurement result. a_1, a_2, and a_3 represent the calibration coefficients, which can be obtained by using three samples with known impedances and applying Cramer's rule. Compared to other de-embedding or calibration methods, the TNC method is relatively easy to use. However, due to the frequency constraint of the IA, the upper-frequency limit is usually up to 120 MHz [131].

The measurement techniques discussed earlier focus on the characterization of EMI filtering chokes under small-signal conditions. However, these chokes may exhibit altered behaviors when subjected to large signal excitations [133]. Deng and See [130] carried out a two-probe setup for measuring the in-circuit impedances of single-phase CMCs by employing an inductive coupling method. However, the mutual coupling between these probes constrained the accuracy beyond 10 MHz [134], [135].

Table IV provides and compares existing measurement methods for determining the impedance/*S*-parameters of EMI filtering chokes, summarizing their key characteristics and differences to highlight the main takeaways. It should be noted that the effective frequency range is derived from the original publications, and the accuracy within this frequency range is quantified using the criteria established in (16).

TABLE IV
COMPARISON OF MEASUREMENT METHODS FOR IMPEDANCE/S-PARAMETERS EXTRACTION OF EMI FILTERING CHOKES

Ref.	Method	Measurement complexity	Versatility		Validated information						Consider parasitics of fixture adapters
			Apparatus	Choke type	Frequency range (Hz)	Accuracy	Data		Mode		
							Mag	Pha	CM	DM	
[76]	Electrically short	Low	VNA	●	100 k – 30 M	N/P					No
[121]		Low	IA	⊜	2 k – 40 M						No
[122]		Low	VNA	⊜	300 k – 20 M						No
[124]	Transmission line theroy	Low	SA	○	500 k – 50 M	High	√			√	Yes
[127]	Two-port circuit de-embedding	High	VNA	○⊜	150 k – 120 M	High	√	√	√	√	Yes
[128]	Single-port circuit de-embedding	High	VNA/IA	●	150 k – 120 M	High	√	√	√	√	Yes
[128]	Three-port network calibration	Moderate	IA	●	150 k – 120 M	High	√	√	√	√	Yes
[129]	Improved open-short-load calibration	Moderate	IA	●	150 k – 30 M	High	√	√	√		Yes
[130]	Inductive coupling method	Moderate	VNA	⊜	100 k – 10 M	High	√		√		Yes

*Acronyms and symbols:
○ Differential-mode choke ⊜ Single-phase common-mode choke ● Three-phase common-mode choke
N/P Not provided Mag Magnitude Pha Phase
CM Common-mode DM Differential-mode IA Impedance analyzer
VNA Vector network analyzer SA Spectrum analyzer

D. Discussions and Recommendations for Characterization Methods of EMI Filtering Chokes

As demonstrated in Sections III-A and B, both analytical and numerical methods remain applicable in the initial design stage before the fabrication of EMI filtering chokes. With the assistance of various commercial simulation software, numerical methods have the capability of characterizing the impedance or *S*-parameters of EMI filtering chokes in a relatively convenient manner. Nonetheless, these platforms are usually expensive and necessitate high computing resources. Furthermore, all these methods require detailed geometrical structures and material properties of chokes, which may not always be available due to intellectual property rights. Measurement methods are more straightforward and have a higher accuracy. However, they require a real product in hand and careful consideration of the parasitics introduced by the fixture adapters.

The extracted impedances or *S*-parameters of EMI filtering chokes can be employed to evaluate mitigation performance and facilitate EMI filter design. Besides, they provide useful insights for choke circuit modeling to achieve systematic EMI simulation, which will be introduced in the following section. In addition, some works cover techniques for assessing other physical characteristics, such as the magnetic field [136], [137], [138], saturation effects [139], [140], [141], thermal analysis [142], etc. These efforts extend beyond the scope of this article and will not be discussed in detail here.

Recommendations for various characterization methods of EMI filtering chokes are summarized as follows.

1) Among all analytical methods, Kovacic et al.'s [94] work is recommended for comprehensive parameter identifications and optimal impedance calculations in single-phase CMCs, while Heldwein et al.'s [77] work is recommended for three-phase CMCs.
2) For numerical methods, Moonen et al.'s [100] work is preferred for wideband impedance characterization of single-phase CMCs. Kovačić et al.'s [66] work is suitable for applications requiring good versatility for both single- and three-phase CMCs. In addition, Kovačević et al.'s [116] work is used for applications necessitating fast simulation speeds.
3) For measurement methods, Jie et al.'s [127] work is recommended for both DMCs and single-phase CMCs, and the work in [128] for three-phase CMCs. Furthermore, Deng and See [130] offer a unique ability for in-circuit characterization of single-phase CMCs under operating conditions.

IV. CIRCUIT MODELING OF EMI FILTERING CHOKES

Leveraging the impedances or *S*-parameters obtained from the characterization of EMI filtering chokes, their circuit models can be constructed. These models provide useful information for EMI prediction and assessment in an entire power electronics system. Depending on the structural characteristics, this section reviews the relevant methods from three categories: distributed, lumped, and multistage circuit models.

A. Distributed Circuit Model

The distributed circuit models of EMI filtering chokes often consist of individual *RLC* parameters for each turn. These *RLC* parameters, which often have well-defined physical meanings, are determined through analytical or numerical characterization methods [66], [94], [97].

Fig. 15 shows a distributed circuit model of a single-phase CMC with N turns per winding, totaling $2N$ turns [94]. To achieve the parametrization process, Kovacic et al. [94] obtained these *RLC* parameters through analytical calculation. This circuit model revealed the inner physical attributes of the choke and facilitated the analysis of localized faults, such as short circuits of winding turns. A similar distributed circuit was employed to model the three-phase CMC using FEM for parameter extraction [97]. However, it neglected the frequency-dependent permeability of nanocrystalline cores and exhibited insufficient accuracy with increasing frequency. To account for the permeability along with the frequency-dependent inductances and improve fitting accuracy, distinct distributed circuit models were constructed at

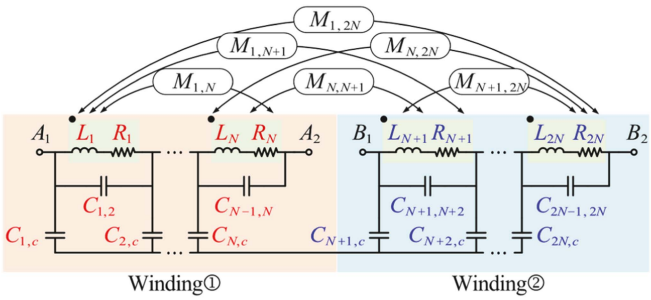

Fig. 15. Distributed circuit model of a single-phase CMC with a total of $2N$ turns [94], where L_l and R_l ($l\epsilon\{1,\ldots,2N\}$) denote the self-inductance and loss of each turn, respectively; $M_{l,m}$ ($l,m\epsilon\{1,\ldots,2N\}$) represents the inductive and resistive mutual coupling between any two turns; $C_{l,m}$ ($l,m\epsilon\{1,\ldots,2N\}$) is the turn-to-turn capacitance and $C_{l,c}$ is the turn-to-core capacitance.

each frequency, as demonstrated in [66]. However, constructing distributed circuit models of EMI filtering chokes is usually time-consuming. Moreover, the *RLC* parameters in these distributed circuit models are often assumed to be constant and frequency-independent [97], whereas they actually vary with frequency. Thus, the applicability of these distributed circuit models is limited for high-frequency EMI evaluation, where the frequency-dependent effects (e.g., skin effect) become nonnegligible and significant.

B. Lumped Circuit Model

As an alternative, lumped circuit models are commonly used for EMI filtering chokes, where the *RLC* parameters can either represent equivalent values with physical meanings or be added solely to enhance the fitting accuracy.

A lumped circuit model for DMC was proposed in [143] for noise filtering studies, as shown in Fig. 16(a). Specifically, L_{eq} denotes the equivalent series inductance, and R_{eq} represents the copper losses in the winding and the magnetic losses in the core. Moreover, C_{eq} is the equivalent parallel capacitance of the winding. All these L_{eq}, R_{eq}, and C_{eq} could be obtained through impedance analysis relying on direct measurements [143] or extracted based on analytical [77] or numerical [144] methods. Considering the significant variation in inductance caused by frequency-dependent permeability and the increased resistance due to the skin and proximity effects, L_{eq} and R_{eq} are replaced by $L_{\text{eq}}(f)$ and $R_{\text{eq}}(f)$, as indicated in Fig. 16(b) [144]. This circuit model can also be employed as a simplified CM or DM circuit for a single-phase CMC [145] or a three-phase CMC [77]. For EMI filtering chokes that exhibit stable inductance across the frequency range of interest, a parallel *RLC* circuit [see Fig. 16(c)] with fixed values could be a more appropriate model. Combined with the circuits of other components within the EMI filter, a detailed coupling analysis can be conducted [146], [147]. Moreover, to improve impedance fitting accuracy, particularly after the first resonant frequency, an additional resistor R_{add} was added in a series with C_{eq}, with its value estimated using a commercial fitting software named 1stOpt [148]. Due to the simplified two-terminal structures, these lumped circuit models [i.e., Fig. 16(a)–(d)] cannot depict the CM and DM behaviors of single- and three-phase CMCs simultaneously. Therefore, they are not applicable to system-level EMI simulations that incorporate power converters, loads, and filters.

To encompass both CM and DM information, several typical lumped circuit models were proposed, as shown in Fig. 16(e)–(g). Liu and Jiang [149] proposed a general procedure to build the high-frequency lumped circuit model of a single-phase ferrite CMC, as depicted in Fig. 16(e). L_{CM}, $C_{\text{t-t}}$, and R_{core} were obtained through the CM impedance measurement setup shown in Fig. 5(b), while others (i.e., L_{leak}, R_{wire}, and $C_{\text{p-p}}$) were derived based on the setups for other types 3 and 5 depicted in Fig. 5(d). Since this method neglected the influences of L_{leak} on CM impedances, the fitting accuracy was limited. As shown in Fig. 16(f), Stevanović and Skibin [150] created a novel circuit configuration of single-phase CMCs, which separated the CM parameters and DM parameters into two *RLC* blocks. L_{CM} and L_{DM} denote the CM and DM inductance of the choke, respectively. R_{CM}, C_{CM}, R_{DM}, and C_{DM} are their respective parallel parameters without actual physical definitions. Relying on the mutual coefficients k_{CM} and k_{DM}, the DM signals could be neglected when only considering CM scenarios and vice versa [150]. All these parameters were assigned values either through the impedance measurements [150] or via the admittance analysis with the measured *S*-parameters [151].

From this circuit configuration, some enhanced models emerged; for example, Ojeda-Rodríguez et al. [75] added phase-to-ground capacitances and modal admittance to facilitate parametrization and improve fitting accuracy relative to the work described in [151]. However, due to the limited number of *RLC* components in these models, they prove inadequate for chokes exhibiting multiresonant impedance behaviors [150]. For a more comprehensive analysis of single-phase CMCs, Kotny et al. [67] proposed a complex lumped circuit model, as illustrated in Fig. 16(g). Specifically, Z_a and Z_b represent the leakage impedance and magnetizing impedance, respectively, while C_i ($i = a, b, c,$ and d) are four capacitors of the choke. Through more than five measurement setups, these parameters were identified based on simplified equivalent circuits and impedance analysis [67]. To better fit the choke characteristics, Z_a and Z_b can be replaced by various *RLC* networks. For facilitating topology selection to ensure precision, an iterative rational function approximation fitting algorithm was proposed [152]. Moreover, several data-driven techniques, including deep neural network, random forest tree, and extreme gradient boosting algorithm (Xgboost), were applied in this circuit configuration for choosing appropriate Z_a or Z_b [153]. These studies (i.e., [67], [152], [153]) provide commendable accuracy and aptly cater to multiresonance scenarios.

For three-phase CMCs, Fig. 16(h) depicts a classic lumped circuit model, where its *RLC* parameters can be derived through admittance analysis with measured *S*-parameters [154]. Instead of using mutual coefficients k_{CM} or k_{DM} to represent the inductive coupling, mutual inductance M was introduced in this circuit. Thus, $L_{\text{self}}+2M$ and $L_{\text{self}}-M$ represent the CM and DM inductances of three-phase CMCs, respectively [154]. Based on the fitting results presented in [154], the maximum magnitude error of S_{21} reached up to 8 dB across the frequency range

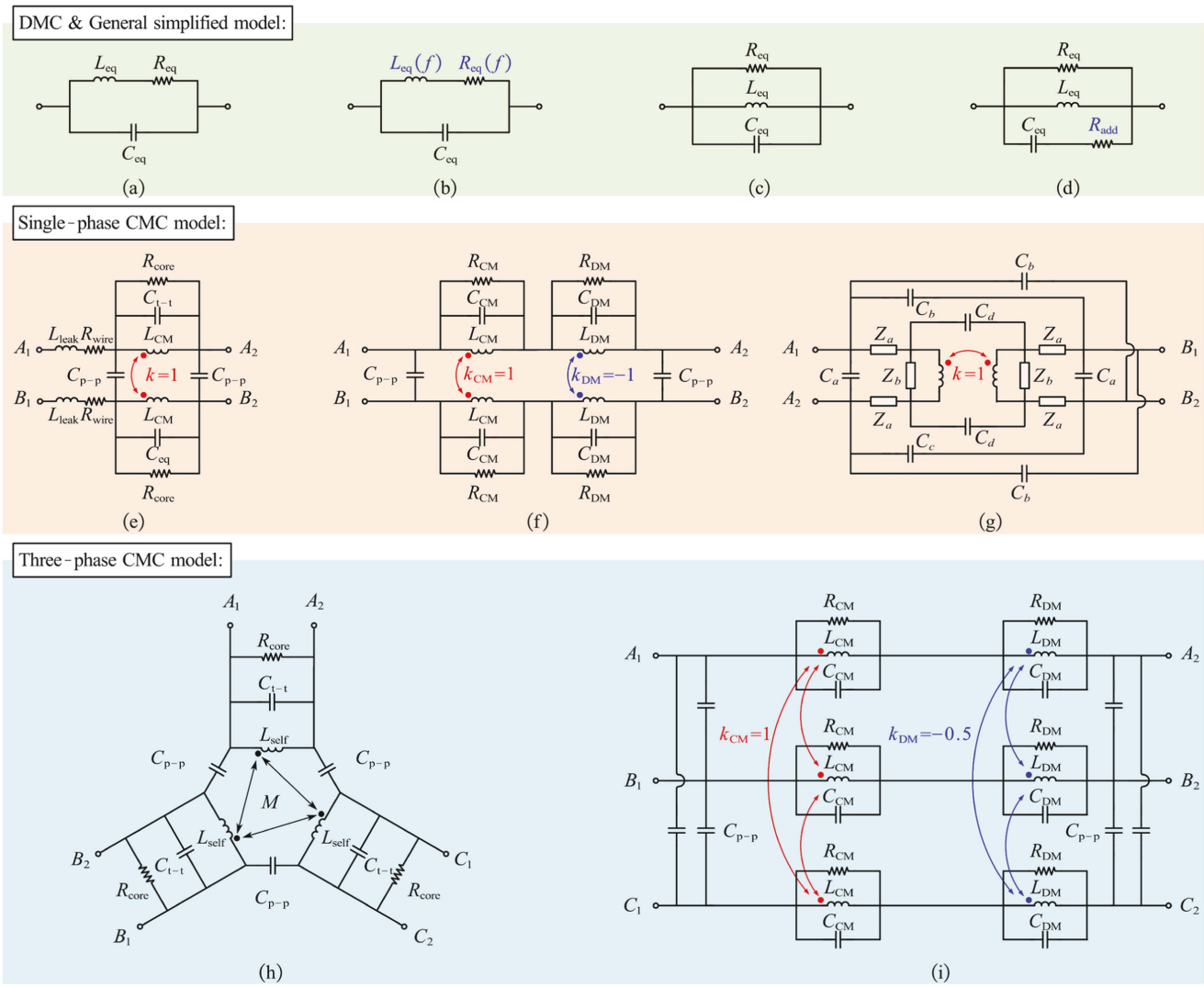

Fig. 16. Typical lumped circuit models for EMI filtering chokes. (a) [143]. (b) [144]. (c) [146]. (d) [148]. (e) [149]. (f) [150]. (g) [67]. (h) [154]. (i) [150].

of 100 kHz to 30 MHz. In addition, phase information was not provided for verification. Stevanović and Skibin [150] also developed a lumped circuit model for three-phase CMCs, as depicted in Fig. 16(i). The parameterization process is similar to that for Fig. 16(f). However, the value of DM mutual coupling coefficients k_{DM} was revised to -0.5 to comply with the three-phase system [150]. Combining the principles of circuit models in Fig. 16(h) and (i) , a modal-parameters circuit model was proposed in [76]. By considering the strong effect of the displacement currents via the high permittivity core, modal admittances were added, finally improving the fitting accuracy compared to that using the circuit model shown in Fig. 16(h).

The *RLC* parameters in Fig. 16(c)–(i) are usually given fixed values in EMI simulation and system analysis. The validity of these lumped circuit models generally relies on the assumption that the inductance influenced by the core permeability remains constant over the frequency range of interest. Therefore, they are effective for most EMI filtering chokes with ferrite cores [151], where the permeability remains rather stable up to several megahertz or even higher. In contrast, chokes with nanocrystalline cores present a challenge for employing these models as they exhibit a high initial permeability which starts to decrease from just a few kilohertz [55], leading to significant frequency-dependent inductances. Due to the merits of low eddy current losses and outstanding permeability [94], the nanocrystalline EMI filtering chokes combine high noise mitigation with a compact size, posing a promising market in the future. Therefore, it is necessary to design appropriate circuit models for them.

C. Multistage Circuit Model

To fit the multiresonance impedance frequency responses or consider the frequency-dependent permeability of a magnetic core used in the chokes, multistage circuit models are often employed. This type of model focuses primarily on the behavior of EMI filtering chokes, where most of the *RLC* parameters are adopted without real physical meanings. Fig. 17 presents several typical multistage circuit models for an overview, and their

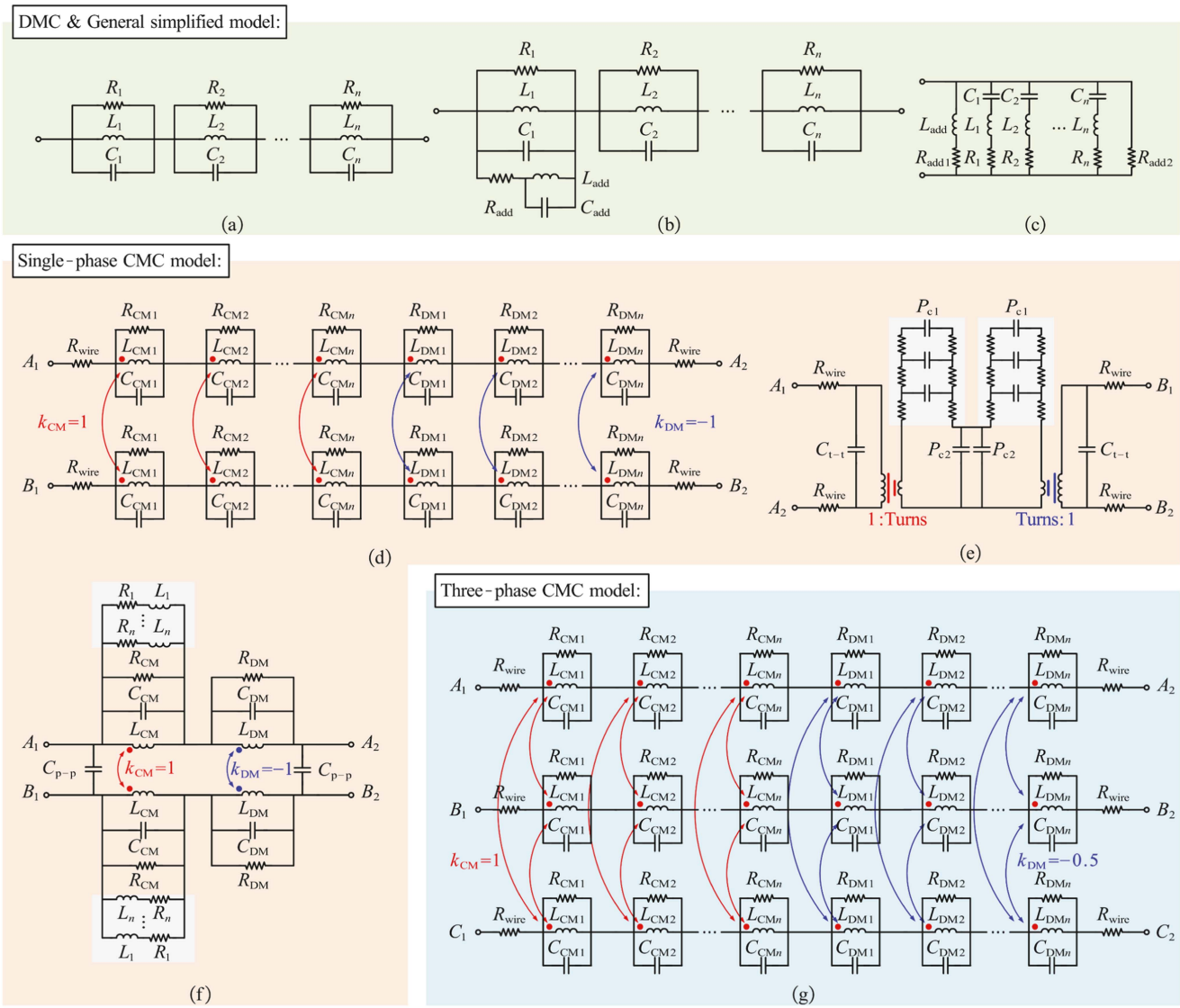

Fig. 17. Typical multistage circuit models for EMI filtering chokes. (a) [155]. (b) [157]. (c) [159]. (d) [160]. (e) [163]. (f) [164]. (g) [160].

features, along with corresponding parameterization methods, are detailed as follows.

A general multistage circuit model was used to encapsulate the impedances of ferrite chokes with multiple resonances [155]. As illustrated in Fig. 17(a), this model consists of several parallel *RLC* blocks connected in series, where R_k, L_k, and C_k represent the elements at the kth stage ($k \in \{1, \ldots, n\}$), and n is defined according to the number of resonances [156]. By conducting impedance measurements, all these *RLC* parameters can be determined by assessing and analyzing the impedance resonance information. To address potential deviations that occur before the first resonant frequency, more *RLC* parameters (i.e., R_{add}, L_{add}, and C_{add}) were added in the first stage to form a new improved Foster model, as shown in Fig. 17(b) [157]. Similarly, these *RLC* parameters were calculated by rational function approximation of the impedance. Chen et al. [158] developed an improved version of the Foster model; nevertheless, the parameterization procedure was not provided. Combined with the AI, Pan et al. [159] applied particle swarm optimization to facilitate parameter extraction of a different circuit model depicted in Fig. 17(c). By properly setting the search range of each unknown parameter, it can achieve high impedance fitting accuracy. All these circuit models [i.e., Fig. 17(a)–(c)] are effective for DMCs. However, due to their two-terminal configurations, they cannot hold both CM and DM behaviors of CMCs simultaneously, and therefore, are not suitable for EMI simulations in an entire system.

For single-phase CMCs, Fig. 17(d) establishes a classic multistage circuit model, which was first proposed in [160]. It was developed from the lumped circuit model shown in Fig. 16(f) and separated the CM and DM blocks [150]. Relying on the CM and DM measurements, their respective *RLC* elements can be calculated via an impedance analysis procedure. In addition, R_{wire}, which usually dominates at low frequencies, can also be derived from the DM impedance information. For realizing the parameter extraction automatically, a genetic algorithm was used for the behavioral modeling of chokes with multiresonances [161]. Unfortunately, this method required expert knowledge to

define the search space of each *RLC* parameter and necessitated multiple fitness functions to avoid degradation [68]. Moreover, Stevanovic et al. [68] also established an approach to handle the nonlinear CM impedance and frequency-dependent CM inductance of a choke with the nanocrystalline core. Nevertheless, a detailed guideline for obtaining the stage number n for such cases was not given, potentially necessitating a trial-and-error process. Following similar multistage circuit models for single-phase CMCs, Jie et al. [104] and Huang et al. [162] provided the analytical-based fitting algorithms for nanocrystalline chokes but also selected n based on the rule of thumb. To address this issue, Jie et al. [102] introduced a concept of the degree of permeability frequency dependence to determine the stage number n, thereby facilitating the parametrization.

There are several other multistage circuit models for single-phase CMCs, such as those shown in Fig. 17(e) [163] and (f) [164]. Takahashi and Ogasawara [163] performed an analogy between the transformer and single-phase chokes, dividing the circuit model into electric (R_{wire} and $C_{\text{t-t}}$) and magnetic (P_{c1} and P_{c2}) parts. Relying on the principles of the proposed permeance-capacitance analogy-based method, multistage RL circuits were assigned in P_{c1} and their values were identified through the real and imaginary parts of permeability (μ' and μ'') [165]. It should be noted that the capacitive elements in this model might be assigned negative values to denote the inductive aspects of the choke's impedance. For instance, P_{c2} could symbolize leakage inductance. It showed a good accuracy of up to 100 MHz, except near the resonant frequency [163]. Considering the limitations of fitting EMI filtering chokes with nanocrystalline cores using the lumped circuit model demonstrated in Fig. 16(f) [151], a series of *RL* elements have been integrated to form a multistage circuit model, as shown in Fig. 17(f) [164]. All these *RLC* parameters in Fig. 17(f) were derived through admittance analysis from the measured S_{21} with CM, DM, and open circuit [i.e., other type 3 in Fig. 5(d)] measurements. This circuit configuration is tailored to precisely adapt to the varying CM inductance caused by the frequency-dependent permeability of a single-phase CMC with a nanocrystalline core. This concept can also be applied in other lumped circuit models as supplements [75], [76].

In addition, Stevanović and Skibin [160] presented another multistage circuit model focusing on the three-phase CMCs with multiresonances. Fig. 17(g) depicts its circuit diagram. By setting the value of k_{DM} at -0.5, the DM signals become negligible in the CM analysis [160]. Moreover, the parameterization process also relied on measurements and impedance analysis [160]. Using the genetic algorithm or analytical-based iteration fitting derivation [102], these multistage circuit models can also be employed for three-phase CMCs with nanocrystalline cores.

D. Discussions and Recommendations of Circuit Modeling Methods for EMI Filtering Chokes

In summary, distributed circuit models delve into the internal physical attributes of an EMI filtering choke, facilitating the initial design prior to choke production. Lumped circuit models, with their simplified structure, can also be employed to analyze the coupling effects between the choke and those nearby EMI filtering components [146]. With more *RLC* elements, they can achieve good impedance fitting for ferrite chokes. Multistage circuit models, focusing predominantly on chokes' behaviors, might not always align with actual physical relevance and can be regarded as "black box" models. These models typically evolve from foundational lumped circuit models, extended or layered with additional *RLC*, *RC*, or *RL* blocks, ultimately fitting the frequency-dependent permeability of nanocrystalline chokes and matching the multiresonances.

Table V compares the existing circuit modeling methods for EMI filtering chokes, including the data source obtained from the choke characterization, parameterization methods for *RLC* identification, studied choke type and related core material, and experimental information used for validation. Similarly, the frequency ranges of these methods are obtained from their respective validation results in each reference, and the accuracy is classified using the criterion in (16). This table serves as a practical resource for engineers and researchers, enabling them to efficiently identify and delve into relevant works to learn and adopt related technologies in a targeted manner.

Except for the techniques outlined in Table V, several other methods have been developed for modeling EMI filtering chokes in some specific applications. Zarei and Khankalantary [166] segmented the CM impedance frequency response of a three-phase CMC into two regions: the inductive region and the frequency-varying inductive-resistive region. These behaviors were modeled using multiple frequency-defined mathematical functions, with the relevant fitting variables determined via a genetic algorithm. According to a similar concept, Nomura et al. [167] and Illia et al. [168] characterized the influence of frequency-dependent permeability as voltage or current sources, allowing these circuits to be used in Simulation Program with Integrated Circuit Emphasis (SPICE [169]) models. To enhance the accuracy of the SPICE circuit model, Cuellar et al. [170] specifically defined the complex permeability of DMCs as a fourth-order diagram and applied a Householder algorithm to identify the parameters. Given that it necessitated to integrate with the high-frequency lossy transmission line, stray capacitance, and wire resistance for impedance fitting, it exhibited considerable complexity compared to multistage circuit models [171].

In addition, a modal model was proposed for analyzing the propagation of CM and DM emissions along with their mode conversion inside a single-phase CMC [172]. This information facilitated to optimize the choke's symmetry design, ultimately enhancing noise mitigation performance in both modes. Dominguez-Palacios et al. [34], [173] modeled the equivalent circuits of single-phase CMCs with conducting surfaces, proposing a smart shielding method to improve choke performance.

Recommendations for various circuit modeling methods for EMI filtering chokes are summarized as follows.

1) For distributed circuit models, Kovačić et al.'s [66] work is recommended as it establishes a detailed process for determining the inner parameters of chokes, aiding in optimizing chokes during the initial design stage.

TABLE V
COMPARISON OF HIGH-FREQUENCY CIRCUIT MODELING METHODS FOR EMI FILTERING CHOKES

Model Category	Ref.	Case studies				Validated information						Parameters are physical defined	Consider multi-resonance
		Parameterization	Information source	Core material	Choke type	Frequency range (Hz)	Accuracy	Data		Mode			
								Mag	Pha	CM	DM		
Distributed	[94]	Analytical	Analytical	△▽	◎●	1 k – 100 M	Low	√				Yes	Yes
	[66]	Numericial	Simulation	▽	◎●	1 k – 100 M	Low	√		√	√	Yes	Yes
	[97]		Simulation	▽	●	1 k – 100 M	Low	√		√	√	Yes	No
Lumped	[144]	Analytical + Numerical	Semi-analytical	▽	○	10 k – 100 M	Low	√	√		√	Yes	No
	[77]	Analytical	Analytical	△▽	●	100 – 100 M	Low	√		√		Yes	No
	[145]		Analytical	△▽	◎	1 k – 100 M	Moderate	√		√		Yes	No
	[67]	Impedance analysis	Measurement	△	◎	1 k – 100 M	Moderate	√	√	√		No	Yes
	[148]		Measurement	△	○	10 k – 30 M	High	√		√		No	No
	[149]		Measurement	△	◎	9 k – 30 M	N/P	√	√	√		Yes	No
	[150]		Measurement	△	◎●	10 k – 30 M	Low	√		√	√	No	No
	[151]	Admittance analysis	Measurement	△	◎	100 k – 50 M	Low	√		√	√	Yes	No
	[154]		Measurement	△	●	100 k – 50 M	Low	√		√	√	Yes	No
	[75]	Modal analysis	Measurement	△	◎	100 k – 100 M	Low	√		√		No	Yes
	[76]		Measurement	△	●	100 k – 30 M	High	√	√	√	√	No	Yes
	[152]	Iterative rational function approximation	Measurement	△	◎	50 – 100 M	High	√		√		No	No
Multi-stage	[68]	Impedance analysis	Measurement	△	◎●	100 – 100 M	High	√		√	√	No	Yes
	[102]		Simulation	▽	◎●	100 – 100 M	High	√	√	√	√	No	No
	[104]		Simulation	▽	◎	10 k – 100 M	High	√	√	√	√	No	No
	[155]		Measurement	N/P	○◎	150 k – 30 M	High	√			√	No	Yes
	[157]		Measurement	△▽	◎	10 k – 30 M	High	√	√	√		No	Yes
	[160]		Measurement	△	◎●	100 – 100 M	High	√		√	√	No	Yes
	[162]		Measurement	▽	◎	100 k – 152 M	Low	√	√	√		No	Yes
	[68]	Genetic algorithm	Measurement	▽	◎	100 – 100 M	High	√		√	√	No	Yes
	[161]		Measurement	△	◎	100 – 100 M	Moderate	√		√	√	No	Yes
	[159]	Particle swarm optimization	Measurement	N/P	○	40 – 110 M	High	√	√		√	No	Yes
	[163]	Permeance-capacitance analogy	Measurement	△▽	◎	1 k – 100 M	High	√	√	√	√	No	No
	[164]	Admittance analysis	Measurement	▽	◎	1 k – 50 M	Moderate	√		√	√	No	No

*Acronyms and symbols:
○ Differential-mode choke
◎ Single-phase common-mode choke
● Three-phase common-mode choke
△ Ferrite core
▽ Nanocrystalline core
N/P Not provided
Mag Magnitude
Pha Phase
CM Common-mode
DM Differential-mode

2) For lumped circuit models, the works presented in [75] and [76] are suggested respectively for single- and three-phase CMCs when the collected data for circuit modeling are *S*-parameters. If the data consist of impedance instead, Tan et al.'s [152] and Heldwein et al.'s [77] works are preferred for single- and three-phase CMCs, respectively.
3) For multistage circuit models, Stevanovic et al. [68] and Jie et al. [102] provided solutions for both single- and three-phase CMCs, which are recommended due to their good accuracy over a wide frequency range.

V. CHALLENGES AND FUTURE TOPICS

The previous sections have provided an in-depth review of the fundamental knowledge, characterization, and circuit modeling of EMI filtering chokes in power electronics. This section will discuss potential challenges and suggest several future topics.

A. Characterizing EMI Filtering Chokes at Higher Frequencies

Referring to Tables I, III, and IV, the current techniques for characterizing EMI filtering chokes typically extend up to

120 MHz, aligning with existing conducted EMI standards for most commercial devices (e.g., CISPR-22 [59]) and electric vehicles (e.g., CISPR-25 [174]). However, this frequency range falls short of encompassing the test requirements for avionics up to 152 MHz (e.g., DO-160 [60]). Moreover, as the trend toward faster switching frequencies in power semiconductor devices continues, significant conducted EMI emissions at higher frequencies are likely to occur, potentially leading to updates in EMC standards [175]. Beyond mitigating conducted EMI noises, EMI filtering chokes are also employed to attenuate radiated EMI emissions [176], [177], [178] and improve the immunity of power electronics devices against intentional EMI attacks [62]. Considering these factors, it is necessary to pursue the characterization of EMI filtering chokes at frequencies over 120 MHz. Thus, potential research topics include:

1) exploring the material behaviors and loss mechanisms of chokes across a wide frequency range;
2) enhancing the integration, acceleration, and optimization of numerical technologies;
3) developing fixture adapters and measurement methods for higher frequencies.

B. Characterization and Modeling of EMI Filtering Chokes in Complex Conditions

Existing works typically focus on the characterization and modeling of EMI filtering chokes under off-circuit conditions, with less emphasis on their performance in real operating conditions, which potentially leads to inaccuracies. Preliminary studies have been conducted, including measuring choke impedances under different feed currents [130], simulating choke losses at elevated temperatures [142], assessing choke performance at high altitudes [179], and evaluating the effects of aging [180]. Building on these foundations, future research could include:

1) developing measurement setups and techniques to characterize the behaviors of chokes under real operating conditions;
2) constructing mathematical and equivalent circuit models for EMI filtering chokes, accounting for saturation effects, temperature variations, and spatial or temporal impacts;
3) building simulation platforms for multiphysics analysis to provide a more comprehensive understanding of choke performance under real-world conditions.

C. Frequency Range Extension and Overall Performance Enhancement

Current core materials and inherent parasitic parameters can limit the attenuation performance of EMI filtering chokes at high frequencies [181]. In addition, when these chokes are assembled into an EMI filter, the coupling between adjacent components may affect the overall filtering effectiveness. To extend the frequency range and enhance the performance of the EMI filters, several promising and effective strategies have been reported. These strategies include optimizing the layouts and structures of choke windings [182], [183], attenuating the parasitic couplings between components [34], [70], canceling parasitic parameters

1) developing novel magnetic core materials with stable and high permeability frequency responses;
2) designing innovative winding manufacturing processes and arrangement strategies to minimize the parasitic parameters within chokes;
3) proposing optimized component layout schemes for EMI filters with constrained planar and spatial requirements, thereby improving their overall performance.

D. AI-Based Applications in EMI Filtering Chokes

The integration of AI technologies with traditional industrial design concepts, particularly in the domain of EMI filtering chokes, is an area of growing interest and potential. Existing works in this field include optimizing component selection [186], offering design guidelines [187], and assisting with parameterization in circuit modeling [68]. However, these applications often necessitate a degree of expert knowledge, which can limit their broader adoption. Looking ahead, there is strong potential for AI techniques to be more deeply woven into the EMC field. Leveraging their robust capabilities, several innovative functionalities could be developed, such as:

1) utilizing an adaptive network and multistage circuit models to enable automated impedance fitting, simplifying the parameterization process;
2) leveraging open databases and resources such as generative pretraining transformer (GPT) series to design EMI filtering chokes, considering component selection, space and weight constraints, winding strategies, etc;
3) integrating with electromagnetic simulation software for multiphysics analysis, ultimately optimizing the layout and packaging of chokes within an EMI filter.

E. Further Explorations on Ongoing Techniques

Many advanced techniques have emerged from the existing characterization and circuit modeling methods to enhance filtering performance or minimize the size and weight of EMI filtering chokes. These innovations offer fresh perspectives on addressing EMI challenges and merit continued exploration. Here, some typical techniques are highlighted, without delving into their details and constraints.

1) Hybrid filtering [19]: employing both active suppression methods and passive components to achieve optimal EMI filter design with reduced size and weight.
2) Magnetic integration [188]: involving customized choke design with one or more shared magnetic cores, aiming to reduce the size and weight of the entire EMI filter.
3) Electromagnetic integration [189]: combining capacitive components to chokes for compact and optimal EMI filter design, usually applying to those types with planar PCB traces or flexible multilayer foils.
4) 3-D printing technique [190]: facilitating flexible designs of the winding and core to enhance the choke's efficiency.

VI. Conclusion

EMI filtering chokes play an integral role in power electron-

extensively studied, focusing on their characterization and circuit modeling for optimization, performance prediction, EMI simulation, and filtering design. To the best of our knowledge, this article provides the first thorough review of the relevant literature on these topics. First of all, the types and structures, operating principles, critical information, and natural modes are introduced for clarity. Subsequently, both characterization and circuit modeling methods for chokes are elaborated, with their related features, case studies, and validated data compared in detail via tables. Finally, inspired by the evolving landscape of power electronics, potential challenges are discussed, and future research topics are suggested. In conclusion, this article aims to provide readers with insights into the principles and technological progress regarding the characterization and circuit modeling of EMI filtering chokes, facilitating targeted searches and selections for related techniques, and encouraging future exploration.

REFERENCES

[1] S. Vazquez et al., "Model predictive control: A review of its applications in power electronics," *IEEE Ind. Electron. Mag.*, vol. 8, no. 1, pp. 16–31, Mar. 2014.

[2] Z. Chen, J. M. Guerrero, and F. Blaabjerg, "A review of the state of the art of power electronics for wind turbines," *IEEE Trans. Power Electron.*, vol. 24, no. 8, pp. 1859–1875, Aug. 2009.

[3] M. Priya, P. Ponnambalam, and K. Muralikumar, "Modular-multilevel converter topologies and applications–A review," *IET Power Electron.*, vol. 12, no. 2, pp. 170–183, Jan. 2019.

[4] C. J. Turner, J. Oyekan, L. Stergioulas, and D. Griffin, "Utilizing industry 4.0 on the construction site: Challenges and opportunities," *IEEE Trans. Ind. Inform.*, vol. 17, no. 2, pp. 746–756, Feb. 2021.

[5] F. Blaabjerg, Y. Yang, K. A. Kim, and J. Rodriguez, "Power electronics technology for large-scale renewable energy generation," *Proc. IEEE*, vol. 111, no. 4, pp. 335–355, Apr. 2023.

[6] F. Blaabjerg, H. Wang, I. Vernica, B. Liu, and P. Davari, "Reliability of power electronic systems for EV/HEV applications," *Proc. IEEE*, vol. 109, no. 6, pp. 1060–1076, Jun. 2021.

[7] A. Hanif, Y. Yu, D. DeVoto, and F. Khan, "A comprehensive review toward the state-of-the-art in failure and lifetime predictions of power electronic devices," *IEEE Trans. Power Electron.*, vol. 34, no. 5, pp. 4729–4746, May 2019.

[8] Z. Ma, S. Wang, Q. Huang, and Y. Yang, "A review of radiated EMI research in power electronics systems," *IEEE J. Emerg. Sel. Topics Power Electron.*, vol. 12, no. 1, pp. 675–694, Feb. 2024.

[9] B. Zhang and S. Wang, "A survey of EMI research in power electronics systems with wide-bandgap semiconductor devices," *IEEE J. Emerg. Sel. Topics Power Electron.*, vol. 8, no. 1, pp. 626–643, Mar. 2020.

[10] C. Li, Q. Ma, Y. Tong, J. Wang, and P. Xu, "A survey of conductive and radiated EMI reduction techniques in power electronics converters across wide-bandgap devices," *IET Power Electron.*, vol. 16, pp. 2121–2137, Jun. 2023.

[11] F. F. Wang, R. Chen, and K. Rajashekara, "Wide bandgap semiconductor-based power electronics for aviation," *IEEE Power Electron. Mag.*, vol. 9, no. 3, pp. 26–36, Sep. 2022.

[12] J. Yao, Y. Lai, Z. Ma, and S. Wang, "Advances in modeling and reduction of conducted and radiated EMI in non-isolated power converters," in *Proc. IEEE Appl. Power Electron. Conf. Expo.*, Phoenix, AZ, USA, 2021, pp. 2305–2312.

[13] Z. Wang et al., "A review of EMI research in modular multilevel converter for HVDC applications," *IEEE Trans. Power Electron.*, vol. 37, no. 12, pp. 14482–14498, Dec. 2022.

[14] N. Jia, L. Xue, and H. Cui, "Mitigating EMI noise in propagation paths: Review of parasitic and coupling effects in power electronic packages, filters, and systems," *IEEE Open J. Power Electron.*, vol. 5, pp. 352–368, 2024.

[15] K. Mainali and R. Oruganti, "Conducted EMI mitigation techniques for switch-mode power converters: A survey," *IEEE Trans. Power Electron.*, vol. 25, no. 9, pp. 2344–2356, Sep. 2010.

[16] S. Tiwari, S. Basu, T. M. Undeland, and O.-M. Midtgård, "Efficiency and conducted EMI evaluation of a single-phase power factor correction boost converter using state-of-the-art SiC MOSFET and SiC diode," *IEEE Trans. Ind. Appl.*, vol. 55, no. 6, pp. 7745–7756, Nov./Dec. 2019.

[17] P. B. Derkacz, J.-L. Schanen, P.-O. Jeannin, P. J. Chrzan, P. Musznicki, and M. Petit, "EMI mitigation of GaN power inverter leg by local shielding techniques," *IEEE Trans. Power Electron.*, vol. 37, no. 10, pp. 11996–12004, Oct. 2022.

[18] Y. Chu and S. Wang, "A generalized common-mode current cancelation approach for power converters," *IEEE Trans. Ind. Electron.*, vol. 62, no. 7, pp. 4130–4140, Jul. 2015.

[19] H. Li, Y. Ding, C. Zhang, Z. Yang, Z. Yang, and B. Zhang, "A compact EMI filter design by reducing the common-mode inductance with chaotic PWM technique," *IEEE Trans. Power Electron.*, vol. 37, no. 1, pp. 473–484, Jan. 2022.

[20] J. Chen, D. Jiang, W. Sun, Z. Shen, and Y. Zhang, "A family of spread-spectrum modulation schemes based on distribution characteristics to reduce conducted EMI for power electronics converters," *IEEE Trans. Ind. Appl.*, vol. 56, no. 5, pp. 5142–5157, Sep./Oct. 2020.

[21] D. Chatterjee and S. K. Mazumder, "EMI mitigation of a Ćuk-based power-electronic system using switching-sequence-based control," *IEEE Trans. Power Electron.*, vol. 36, no. 9, pp. 10627–10644, Sep. 2021.

[22] R. H. Ashique and Z. Salam, "A family of true zero voltage zero current switching (ZVZCS) nonisolated bidirectional DC–DC converter with wide soft switching range," *IEEE Trans. Ind. Electron.*, vol. 64, no. 7, pp. 5416–5427, Jul. 2017.

[23] F. Fiori, "On the use of magnetically coupled resonant snubbers to mitigate the electromagnetic emission of power switching circuits," *IEEE Trans. Electromagn. Compat.*, vol. 64, no. 1, pp. 259–262, Feb. 2022.

[24] W.-W. Yen and P. C.-P. Chao, "A ZVS phase-shift full-bridge converter with input current steering to reduce EMI noise," *IEEE Trans. Power Electron.*, vol. 37, no. 10, pp. 11937–11950, Oct. 2022.

[25] S. Xu, S. Xu, D. Xu, Q. Qian, W. Sun, and J. Zhu, "A review on recent effort of conductive EMI suppression methods in high-frequency power converters," *IET Power Electron.*, vol. 15, no. 16, pp. 1921–1935, Jun. 2022.

[26] R. Goswami and S. Wang, "Modeling and stability analysis of active differential-mode EMI filters for AC/DC power converters," *IEEE Trans. Power Electron.*, vol. 33, no. 12, pp. 10277–10291, Dec. 2018.

[27] Y. Zhou et al., "A new integrated active EMI filter topology with both CM noise and DM noise attenuation," *IEEE Trans. Power Electron.*, vol. 37, no. 5, pp. 5466–5478, May 2022.

[28] Y. Zhang, Q. Li, and D. Jiang, "A motor CM impedance based transformerless active EMI filter for DC-side common-mode EMI suppression in motor drive system," *IEEE Trans. Power Electron.*, vol. 35, no. 10, pp. 10238–10248, Oct. 2020.

[29] B. Narayanasamy and F. Luo, "A survey of active EMI filters for conducted EMI noise reduction in power electronic converters," *IEEE Trans. Electromagn. Compat.*, vol. 61, no. 6, pp. 2040–2049, Dec. 2019.

[30] Y. Liu, X. Zhang, Z. Lu, and J. Yin, "Design of planar magnetic integrated LCL-EMI hybrid filter for the grid-connected inverter," *IEEE Trans. Ind. Appl.*, vol. 60, no. 3, pp. 4280–4291, May/Jun. 2024.

[31] J. Biela, A. Wirthmueller, R. Waespe, M. L. Heldwein, K. Raggl, and J. W. Kolar, "Passive and active hybrid integrated EMI filters," *IEEE Trans. Power Electron.*, vol. 24, no. 5, pp. 1340–1349, May 2009.

[32] M. Ali, E. Labouré, F. Costa, and B. Revol, "Design of a hybrid integrated EMC filter for a DC–DC power converter," *IEEE Trans. Power Electron.*, vol. 27, no. 11, pp. 4380–4390, Nov. 2012.

[33] V. Tarateeraseth, "EMI filter design: Part III: Selection of filter topology for optimal performance," *IEEE Electromagn. Compat. Mag.*, vol. 1, no. 2, pp. 60–73, Second Quarter 2012.

[34] C. Domínguez-Palacios, P. González-Vizuete, M. A. Martín-Prats, and J. B. Mendez, "Smart shielding techniques for common mode chokes in EMI filters," *IEEE Trans. Electromagn. Compat.*, vol. 61, no. 4, pp. 1329–1336, Aug. 2019.

[35] F. Fan, K. Y. See, X. Liu, K. Li, and A. K. Gupta, "Systematic common-mode filter design for inverter-driven motor system based on in-circuit impedance extraction," *IEEE Trans. Electromagn. Compat.*, vol. 62, no. 5, pp. 1711–1722, Oct. 2020.

[36] S. Wang, F. C. Lee, and W. G. Odendaal, "Characterization and parasitic extraction of EMI filters using scattering parameters," *IEEE Trans. Power Electron.*, vol. 20, no. 2, pp. 502–510, Mar. 2005.

[37] Y. Liu, K. Y. See, S. Yin, R. Simanjorang, A. K. Gupta, and J.-S. Lai, "Equivalent circuit model of high power density SiC converter for common-mode conducted emission prediction and analysis," *IEEE Electromagn. Compat. Mag.*, vol. 8, no. 1, pp. 67–74, First Quarter 2019.

[38] R. Lai, Y. Maillet, F. Wang, S. Wang, R. Burgos, and D. Boroyevich, "An integrated EMI choke for differential-mode and common-mode noise suppression," *IEEE Trans. Power Electron.*, vol. 25, no. 3, pp. 539–544, Mar. 2010.

[39] D. O. Boillat, F. Krismer, and J. W. Kolar, "EMI filter volume minimization of a three-phase, three-level T-type PWM converter system," *IEEE Trans. Power Electron.*, vol. 32, no. 4, pp. 2473–2480, Apr. 2017.

[40] W. Tan, C. Cuellar, X. Margueron, and N. Idir, "A common-mode choke using toroid-EQ mixed structure," *IEEE Trans. Power Electron.*, vol. 28, no. 1, pp. 31–35, Jan. 2013.

[41] M. Kącki, M. S. Rylko, J. G. Hayes, and C. R. Sullivan, "Magnetic material selection for EMI filters," in *Proc. IEEE Energy Convers. Congr. Expo.*, Cincinnati, OH, USA, 2017, pp. 2350–2356.

[42] R. Suárez, M. Tijero, R. Moreno, A. Arriola, and J. M. González, "3-D modeling and characterization of ferrite and nanocrystalline magnetic cores for EMI applications," in *Proc. IEEE Int. Symp. Electromagn. Compat. Signal Power Integr.*, 2023, pp. 28–33.

[43] S. Takahashi, S. Ogasawara, M. Takemoto, K. Orikawa, and M. Tamate, "Experimental evaluation of the relationship between filter inductor impedances and dimensional resonances of MnZn ferrites," in *Proc. IEEE 4th Int. Future Energy Electron. Conf.*, 2019, pp. 1–8.

[44] H. Zhang and S. Wang, "Near magnetic field assessment and reduction for magnetic inductors with magnetic moment analysis," *IEEE Trans. Power Electron.*, vol. 37, no. 2, pp. 1641–1652, Feb. 2022.

[45] Y. Yang, M. Mu, Z. Liu, F. C. Lee, and Q. Li, "Common mode EMI reduction technique for interleaved MHz critical mode PFC converter with coupled inductor," in *Proc. IEEE Energy Convers. Congr. Expo.*, 2015, pp. 233–239.

[46] Y. Liu, S. Jiang, W. Liang, H. Wang, and J. Peng, "Modeling and design of the magnetic integration of single-and multi-stage EMI filters," *IEEE Trans. Power Electron.*, vol. 35, no. 1, pp. 276–288, Jan. 2020.

[47] J. Ma, W. Zhong, P. Chen, Y. Chen, and D. Xu, "An optimization design of output filter in a grid connected inverter with flexible multilayer foil technique," *IEEE Trans. Energy Convers.*, vol. 34, no. 1, pp. 221–231, Mar. 2019.

[48] S. Wang and C. Xu, "Extraction of magnetic parameters for elements of a planar EMI filter," *IEEE Trans. Electromagn. Compat.*, vol. 56, no. 2, pp. 360–366, Apr. 2014.

[49] S. Jiang, P. Wang, W. Wang, and D. Xu, "Modeling and design of full electromagnetic integration of a symmetrical EMI filtering circuit with flexible multi-layer foil technique," *IEEE Trans. Electromagn. Compat.*, vol. 65, no. 2, pp. 414–424, Apr. 2023.

[50] K. Y. See and J. Deng, "Measurement of noise source impedance of SMPS using a two probes approach," *IEEE Trans. Power Electron.*, vol. 19, no. 3, pp. 862–868, May 2004.

[51] R. L. Ozenbaugh and T. M. Pullen, *EMI Filter Design*. New York, NY, USA: CRC Press, 2000, pp. 25–27.

[52] K. Raggl, T. Nussbaumer, and J. W. Kolar, "Guideline for a simplified differential-mode EMI filter design," *IEEE Trans. Ind. Electron.*, vol. 57, no. 3, pp. 1031–1040, Mar. 2010.

[53] S. Wang, Y. Y. Maillet, F. Wang, R. Lai, F. Luo, and D. Boroyevich, "Parasitic effects of grounding paths on common-mode EMI filter's performance in power electronics systems," *IEEE Trans. Ind. Electron.*, vol. 57, no. 9, pp. 3050–3059, Sep. 2010.

[54] M. J. Nave, "On modeling the common mode inductor," in *Proc. IEEE Int. Symp. Electromagn. Compat.*, 1991, pp. 452–457.

[55] R. Ren, Z. Dong, B. Liu, and F. Wang, "Impedance-based common-mode inductor design approach considering frequency-dependent and imaginary permeability," in *Proc. IEEE Appl. Power Electron. Conf. Expo.*, New Orleans, LA, USA, 2020, pp. 2680–2686.

[56] R. Chen, J. D. Van Wyk, S. Wang, and W. G. Odendaal, "Improving the characteristics of integrated EMI filters by embedded conductive layers," *IEEE Trans. Power Electron.*, vol. 20, no. 3, pp. 611–619, May 2005.

[57] D. Jiang, R. Lai, F. Wang, F. Luo, S. Wang, and D. Boroyevich, "Study of conducted EMI reduction for three-phase active front-end rectifier," *IEEE Trans. Power Electron.*, vol. 26, no. 12, pp. 3823–3831, Dec. 2011.

[58] Y. Li and S. Wang, "Modeling and increasing the high-frequency impedance of single-layer Mn-Zn ferrite toroidal inductors with electromagnetic analysis," *IEEE Trans. Power Electron.*, vol. 36, no. 6, pp. 6943–6953, Jun. 2021.

[59] *Radio Disturbance Characteristics-Limits and Methods of Measurement*, British Standards, London, U.K., 2010. [Online]. Available: https://bsol.bsigroup.com

[60] "Environmental Conditions and Test Procedures for Airborne Equipment," *RTCA, Inc., Document RTCA/DO-160E Book, U.S. States standards*, 2005. [Online]. Available: https://do160.org

[61] J. Yao, Y. Li, S. Wang, X. Huang, and X. Lyu, "Modeling and reduction of radiated EMI in a GaN IC-based active clamp flyback adapter," *IEEE Trans. Power Electron.*, vol. 36, no. 5, pp. 5440–5449, May 2021.

[62] H. Jie et al., "A review of intentional electromagnetic interference in power electronics: Conducted and radiated susceptibility," *IET Power Electron.*, vol. 17, pp. 1487–1506, Mar. 2024, doi: 10.1049/pel2.12685.

[63] V. Tarateeraseth, K. Y. See, F. G. Canavero, and R. W.-Y. Chang, "Systematic electromagnetic interference filter design based on information from in-circuit impedance measurements," *IEEE Trans. Electromagn. Compat.*, vol. 52, no. 3, pp. 588–598, Aug. 2010.

[64] *Requirements for the Control of Electromagnetic Interference Characteristics of Subsystems and Equipment*, MIL-STD-461G, Dept. Defense Interface Standard, 2015.

[65] S. Wang, Y. Y. Maillet, F. Wang, D. Boroyevich, and R. Burgos, "Investigation of hybrid EMI filters for common-mode EMI suppression in a motor drive system," *IEEE Trans. Power Electron.*, vol. 25, no. 4, pp. 1034–1045, Apr. 2010.

[66] M. Kovačić, S. Stipetić, Z. Hanić, and D. Žarko, "Small-signal calculation of common-mode choke characteristics using finite-element method," *IEEE Trans. Electromagn. Compat.*, vol. 57, no. 1, pp. 93–101, Feb. 2015.

[67] J.-L. Kotny, X. Margueron, and N. Idir, "High-frequency model of the coupled inductors used in EMI filters," *IEEE Trans. Power Electron.*, vol. 27, no. 6, pp. 2805–2812, Jun. 2012.

[68] I. Stevanovic, S. Skibin, M. Masti, and M. Laitinen, "Behavioral modeling of chokes for EMI simulations in power electronics," *IEEE Trans. Power Electron.*, vol. 28, no. 2, pp. 695–705, Feb. 2013.

[69] Z. Zhao et al., "Physics informed neural network-based high-frequency modeling of induction motors," *Chin. J. Electr. Eng.*, vol. 8, no. 4, pp. 30–38, Dec. 2022.

[70] P. Gonzalez-Vizuete, J. Bernal-Mendez, M. J. Freire, and M. A. Martin-Prats, "Improving performance of compact EMI filters by using metallic and ferrite sheets," *IEEE Trans. Power Electron.*, vol. 36, no. 8, pp. 9057–9068, Aug. 2021.

[71] D. M. Pozar, *Microwave Engineering*. Hoboken, NJ, USA: Wiley, 2012.

[72] H. Jie, Z. Zhao, F. Fei, R. Simanjorang, F. Sasongko, and K. Y. See, "A survey of impedance measurement methods in power electronics," in *Proc. IEEE Int. Instrum. Meas. Technol. Conf.*, 2022, pp. 1–6.

[73] K. R. Li, K. Y. See, and X. M. Li, "Inductive coupled in-circuit impedance monitoring of electrical system using two-port ABCD network approach," *IEEE Trans. Instrum. Meas.*, vol. 64, no. 9, pp. 2489–2495, Sep. 2015.

[74] C. R. Paul, *Introduction to Electromagnetic Compatibility*, 2nd ed. Hoboken, NJ, USA: Wiley, 2006.

[75] A. Ojeda-Rodríguez, J. Bernal-Méndez, and M. Martín-Prats, "Modal theory and approach for accurate characterization of common mode chokes," *IEEE Trans. Power Electron.*, vol. 38, no. 9, pp. 10516–10529, Sep. 2023.

[76] Á. Ojeda-Rodríguez, C. Domínguez-Palacios, J. B. Mendez, and M. A. Martín-Prats, "Analyzing and characterizing common mode chokes for three phase systems," *IEEE Trans. Power Electron.*, vol. 39, no. 5, pp. 4916–4932, May 2024.

[77] M. L. Heldwein, L. Dalessandro, and J. W. Kolar, "The three-phase common-mode inductor: Modeling and design issues," *IEEE Trans. Ind. Electron.*, vol. 58, no. 8, pp. 3264–3274, Aug. 2011.

[78] K. Küpfmüller, W. Mathis, and A. Reibiger, *Theoretische Elektrotechnik*. Berlin, Germany: Springer, 2013.

[79] L. Middelstädt, S. Skibin, R. Döbbelin, and A. Lindemann, "Analytical determination of the first resonant frequency of differential mode chokes by detailed analysis of parasitic capacitances," in *Proc. 16th Eur. Conf. Power Electron. Appl.*, 2014, pp. 1–10.

[80] M. K. Kazimierczuk, *High-Frequency Magnetic Components*. Hoboken, NJ, USA: Wiley, 2014.

[81] A. Massarini and M. K. Kazimierczuk, "Self-capacitance of inductors," *IEEE Trans. Power Electron.*, vol. 12, no. 4, pp. 671–676, Jul. 1997.

[82] S. W. Pasko, M. K. Kazimierczuk, and B. Grzesik, "Self-capacitance of coupled toroidal inductors for EMI filters," *IEEE Trans. Electromagn. Compat.*, vol. 57, no. 2, pp. 216–223, Apr. 2015.

[83] G. Dong, F. Zhang, Y. Liu, W. Meng, and C. Xu, "Analytical method for extraction of stray capacitance in single-layer CM chokes," in *Proc. IEEE Energy Convers. Congr. Expo.*, 2019, pp. 3185–3191.

[84] M. Ali, R. Bushra, M. Magdowski, R. Vick, J. Friebe, and A. Mertens, "Prediction of stray capacitance of CM chokes and its influence on EMI filters," in *Proc. PCIM Europe; Int. Exhib. Conf. Power Electron., Intell. Motion, Renewable Energy Energy Manage.*, 2022, pp. 1–10.

[85] Q. Li, B. Xie, Y. Zhang, J. Ma, and C. Yuan, "A general analytical model of single-layer common-mode chokes," *IEEE Trans. Power Electron.*, vol. 39, no. 6, pp. 6591–6596, Mar. 2024.

[86] Y. Li, J. Yao, and S. Wang, "Increase high frequency impedance of ferrite toroid inductors based on electromagnetic energy analysis," in *Proc. IEEE Energy Convers. Congr. Expo.*, 2019, pp. 6184–6191.

[87] B. Liu, R. Ren, F. Wang, D. Costinett, and Z. Zhang, "Winding scheme with fractional layer for differential-mode toroidal inductor," *IEEE Trans. Ind. Electron.*, vol. 67, no. 2, pp. 1592–1604, Feb. 2020.

[88] A. Muetze, "Scaling issues for common-mode chokes to mitigate ground currents in inverter-based drive systems," *IEEE Trans. Ind. Appl.*, vol. 45, no. 1, pp. 286–294, Jan./Feb. 2009.

[89] A. Massarini, M. Kazimierczuk, and G. Grandi, "Lumped parameter models for single- and multiple-layer inductors," in *Proc. 27th Annu. IEEE Power Electron. Spec. Conf.*, 1996, vol. 1, pp. 295–301.

[90] S. Takahashi, S. Ogasawra, M. Takemoto, K. Orikawa, and M. Tamate, "A modeling technique for designing high-frequency three-phase common-mode inductors," in *Proc. IEEE Energy Convers. Congr. Expo.*, 2018, pp. 6600–6606.

[91] C. Cuellar, W. Tan, X. Margueron, A. Benabou, and N. Idir, "Measurement method of the complex magnetic permeability of ferrites in high frequency," in *Proc. IEEE Int. Instrum. Meas. Technol. Conf. Proc.*, Graz, Austria, 2012, pp. 63–68.

[92] J. Xue and F. Wang, "Modeling and design of common-mode inductor for conductive EMI noise suppression in DC-fed motor drive system," in *Proc. IEEE Energy Convers. Congr. Expo.*, 2012, pp. 645–651.

[93] D. Han, C. T. Morris, W. Lee, and B. Sarlioglu, "Three-phase common mode inductor design and size minimization," in *Proc. IEEE Transp. Electrific. Conf. Expo.*, 2016, pp. 1–8.

[94] M. Kovacic, Z. Hanic, S. Stipetic, S. Krishnamurthy, and D. Zarko, "Analytical wideband model of a common-mode choke," *IEEE Trans. Power Electron.*, vol. 27, no. 7, pp. 3173–3185, Jul. 2012.

[95] M. Bartoli, A. Reatti, and M. Kazimierczuk, "Modelling iron-powder inductors at high frequencies," in *Proc. IEEE Ind. Appl. Soc. Annu. Meeting*, 1994, vol. 2, pp. 1225–1232.

[96] A. Mu, L. D. Angulo, A. Gasc, K. Tekbas, R. Moreno, and S. G. Garcia, "Impedance modelling of common mode ferrite chokes using transmission line theory," *IEEE Trans. Power Electron.*, vol. 39, no. 4, pp. 4224–4233, Apr. 2024.

[97] Y. Liu et al., "FEM modelling of three-phase common mode choke for performance evaluation," in *Proc. Asia-Pac. Int. Symp. Electromagn. Compat.*, Shenzhen, China, 2016, pp. 96–99.

[98] Y. Zhang and D. Jiang, "A lumped common mode choke model by finite element software considering complex permeability change with frequency," in *Proc. IEEE Int. Power Electron. Appl. Conf. Expo.*, 2018, pp. 1–4.

[99] A. Bingler, B. Pintér, K. Marák, S. Bilicz, and M. Csörnyei, "Surrogate model based parameter identification for 3D modeling of common mode chokes," *IEEE Trans. Magn.*, vol. 60, no. 3, Mar. 2024, Art. no. 8400604.

[100] N. Moonen, R. Vogt-Ardatjew, A. Roc'h, and F. Leferink, "3-D full-wave high frequency common mode choke modeling," *IEEE Trans. Electromagn. Compat.*, vol. 62, no. 3, pp. 707–714, Jun. 2020.

[101] H. Jie et al., "Investigation on phase sensitivity unveiling of finite-element analysis modelled single-phase common-mode chokes," in *Proc. 49th Annu. Conf. IEEE Ind. Electron. Soc.*, 2023, pp. 1–6.

[102] H. Jie et al., "High-frequency impedance modeling of nanocrystalline common-mode chokes using mixed-mode theory and improved multi-stage RLC iteration circuit," *IEEE Trans. Ind. Electron.*, early access, Aug. 2024, doi: 10.1109/TIE.2024.3429642.

[103] R. He et al., "Modeling strategy for EMI filters," *IEEE Trans. Electromagn. Compat.*, vol. 62, no. 4, pp. 1572–1581, Aug. 2020.

[104] H. Jie et al., "Characterization and modeling of single-phase common-mode chokes via finite-element analysis," in *Proc. 49th Annu. Conf. IEEE Ind. Electron. Soc.*, 2023, pp. 1–6.

[105] Z. Dong, R. Ren, B. Liu, and F. Wang, "Data-driven leakage inductance modeling of common mode chokes," in *Proc. IEEE Energy Convers. Congr. Expo.*, 2019, pp. 6641–6646.

[106] Q. Yu and T. W. Holmes, "A study on stray capacitance modeling of inductors by using the finite element method," *IEEE Trans. Electromagn. Compat.*, vol. 43, no. 1, pp. 88–93, Feb. 2001.

[107] B. Xie, Q. Li, Y. Zhang, Z. Zhang, and Q. Luo, "Improved quantitative analysis method for extracting stray capacitance in common-mode inductor based on finite elements," in *Proc. 26th Int. Conf. Electr. Mach. Syst.*, 2023, pp. 4395–4400.

[108] F. Salomez, A. Videt, and N. Idir, "Modelling and minimization of the parasitic capacitance of ring core inductors," in *Proc. 23rd Eur. Conf. Power Electron. Appl.*, 2021, pp. 1–10.

[109] F. Salomez, A. Videt, and N. Idir, "Modeling and minimization of the parasitic capacitances of single-layer toroidal inductors," *IEEE Trans. Power Electron.*, vol. 37, no. 10, pp. 12426–12436, Oct. 2022.

[110] A. Taflove, A. Oskooi, and S. G. Johnson, *Advances in FDTD Computational Electrodynamics: Photonics and Nanotechnology*. Norwood, MA, USA: Artech House, 2013.

[111] A. G. Bravo et al., "Time domain simulation of common mode ferrite chokes at system level," *IEEE Trans. Electromagn. Compat.*, vol. 65, no. 6, pp. 1900–1908, Dec. 2023.

[112] I. Kovačević, A. Müsing, and J. W. Kolar, "PEEC modelling of toroidal magnetic inductor in frequency domain," in *Proc. Power Electron. Conf.*, 2010, pp. 3158–3165.

[113] D. Eremyan, A. Gheonjian, D. Imnadze, K. Parshutkin, and R. Jobava, "PEEC-based wideband micro-model of inductive components for power electronics applications," in *Proc. Int. Symp. Electromagn. Compat.*, 2023, pp. 1–6.

[114] I. F. Kovačević, A. M. Müsing, and J. W. Kolar, "An extension of PEEC method for magnetic materials modeling in frequency domain," *IEEE Trans. Magn.*, vol. 47, no. 5, pp. 910–913, May 2011.

[115] I. F. Kovačević, T. Friedli, A. M. Müsing, and J. W. Kolar, "Full PEEC modeling of EMI filter inductors in the frequency domain," *IEEE Trans. Magn.*, vol. 49, no. 10, pp. 5248–5256, Oct. 2013.

[116] I. F. Kovačević, T. Friedli, A. M. Müsing, and J. W. Kolar, "3-D electromagnetic modeling of parasitics and mutual coupling in EMI filters," *IEEE Trans. Power Electron.*, vol. 29, no. 1, pp. 135–149, Jan. 2014.

[117] I. F. Kovačević, T. Friedli, A. M. Muesing, and J. W. Kolar, "3-D electromagnetic modeling of EMI input filters," *IEEE Trans. Ind. Electron.*, vol. 61, no. 1, pp. 231–242, Jan. 2014.

[118] "R&S LCX LCR METER: The top-class in component testing," Rohde&Schwarz, Munich, Germany, 2023. [Online]. Available: https://scdn.rohde-schwarz.com/ur/pws/dl_downloads/dl_common_library/dl_brochures_and_datasheets/pdf_1/LCX_dat_en_3609-8309-32_v0201.pdf

[119] "Accessories catalog for impedance measurements," Keysight Technol., Santa Rosa, CA, USA, 2017. [Online]. Available: https://www.keysight.com/sg/en/assets/7018-06727/brochures/5965-4792.pdf

[120] A. Roc'h, H. Bergsma, D. Zhao, B. Ferreira, and F. Leferink, "Comparison of evaluated and measured performances of common mode chokes," in *Proc. Int. Symp. Electromagn. Compat. Eur.*, Hamburg, Germany, Sep. 2008, pp. 1–5.

[121] A. Roc'h and F. Leferink, "Optimization of the in situ performance of common mode chokes for power drive systems using designable parameters," *IEEE Trans. Electromagn. Compat.*, vol. 60, no. 2, pp. 529–535, Apr. 2018.

[122] P. Hu et al., "A simple measurement method for frequency-dependent impedance and parasitic parameters of common-mode chokes," in *Proc. IEEE Int. Symp. Electromagn. Compat., Signal Power Integr.*, New Orleans, LA, USA, 2019, pp. 266–271.

[123] K. Kostov and J. Kyyra, "Common-mode choke coils characterization," in *Proc. 13th Eur. Conf. Power Electron. Appl.*, 2009, pp. 1–9.

[124] J. B. Mendez, M. J. Freire, and M. A. M. Prats, "Overcoming the effect of test fixtures on the measurement of parasitics of capacitors and inductors," *IEEE Trans. Power Electron.*, vol. 35, no. 1, pp. 15–19, Jan. 2020.

[125] H. Jie et al., "Customized test fixture for accurate impedance measurement of EMI filtering chokes," in *Proc. Asia-Pac. Int. Symp. Electromagn. Compat.*, 2022, pp. 216–218.

[126] H. Jie et al., "Customized fixture adapter for accurate CM choke impedance measurement up to 100 MHz," in *Proc. IEEE 4th Int. Conf. Smart Power Internet Energy Syst.*, Dec. 2022, pp. 76–80.

[127] H. Jie et al., "VNA-based fixture adapters for wideband accurate impedance extraction of single-phase EMI filtering chokes," *IEEE Trans. Ind. Electron.*, vol. 70, no. 8, pp. 7821–7831, Aug. 2023.

[128] H. Jie et al., "High-precision broadband impedance measurements of three-phase common-mode chokes using single-port circuit de-embedding and three-port network calibration methods," *IEEE Trans. Ind. Electron.*, vol. 71, no. 8, pp. 8248–8258, Aug. 2024.

[129] H. Jie et al., "Impedance measurement of three-phase common-mode chokes in power electronic applications," in *Proc. IEEE Int. Instrum. Meas. Technol. Conf.*, Kuala Lumpur, Malaysia, May 2023, pp. 1–6.

[130] J. Deng and K. Y. See, "In-circuit characterization of common-mode chokes," *IEEE Trans. Electromagn. Compat.*, vol. 49, no. 2, pp. 451–454, May 2007.
[131] "E4990A Impedance Analyzer, 20 Hz to 10/20/30/50/120 MHz," Keysight Technol., Santa Rosa, CA, USA, 2021. [Online] Available: [Online]. Available: https://www.keysight.com/sg/en/support/E4990A/impedance-analyzer-20-hz-10-20-30-50-120-mhz.html
[132] Z. Zhao, A. Weerasinghe, Q. Sun, F. Fan, and K. Y. See, "Improved calibration technique for two-probe setup to enhance its in-circuit impedance measurement accuracy," *Measurement*, vol. 185, Nov. 2021, Art. no. 110007.
[133] D. Nemashkalo, P. Koch, N. Moonen, and F. Leferink, "Unexpected common mode choke saturation," in *Proc. Int. Symp. Electromagn. Compat.*, Sep. 2023, pp. 1–5.
[134] Z. Zhao, "Measurement setup consideration and implementation for inductively coupled online impedance extraction," Ph.D. dissertation, School Electr. Electron. Eng., Nanyang Tech. Univ., Singapore, 2021.
[135] Z. Zhao et al., "In-circuit impedance measurement setups of inductive coupling approach: A review," in *Proc. Asia-Pac. Int. Symp. Electromagn. Compat.*, Beijing, China, Sep. 2022, pp. 228–230.
[136] Y. Lai, S. Wang, and B. Zhang, "Investigation of magnetic field immunity and near magnetic field reduction for the inductors in high power density design," *IEEE Trans. Power Electron.*, vol. 34, no. 6, pp. 5340–5351, Jun. 2019.
[137] B. Zhang and S. Wang, "Analysis and reduction of the near magnetic field emission from toroidal inductors," *IEEE Trans. Power Electron.*, vol. 35, no. 6, pp. 6251–6268, Jun. 2020.
[138] Y. Lai, S. Wang, Y. Yang, Q. Huang, and Z. Ma, "Review on modeling and emissions from EMI filters in power electronics: Inductors," in *Proc. IEEE Symp. Electromagn. Compat. Signal Power Integr.*, Aug. 2023, pp. 566–572.
[139] H. Chen, Z. Qian, S. Yang, and C. Wolf, "Finite-element modeling of saturation effect excited by differential-mode current in a common-mode choke," *IEEE Trans. Power Electron.*, vol. 24, no. 3, pp. 873–877, Mar. 2009.
[140] R. Salas and J. Pleite, "Equivalent electrical model of a ferrite core inductor excited by a square waveform including saturation and power losses for circuit simulation," *IEEE Trans. Magn.*, vol. 49, no. 7, pp. 4257–4260, Jul. 2013.
[141] B. Wunsch, S. Skibin, V. Forsstrom, and T. Christen, "Broadband modeling of magnetic components with saturation and hysteresis for circuit simulations of power converters," *IEEE Trans. Magn.*, vol. 54, no. 11, Nov. 2018, Art. no. 7301505.
[142] Y. Liu, K. Y. See, and R. Simanjorang, "3-D modeling of common mode choke for thermal analysis," in *Proc. Asia–Pacific Int. Symp. Electromagn. Compat.*, 2017, pp. 79–81.
[143] Q. Yu, T. W. Holmes, and K. Naishadham, "RF equivalent circuit modeling of ferrite-core inductors and characterization of core materials," *IEEE Trans. Electromagn. Compat.*, vol. 44, no. 1, pp. 258–262, Feb. 2002.
[144] F. Salomez, A. Videt, and N. Idir, "Semi-analytical model of parasitic capacitance of inductor with conductive core," in *Proc. PCIM Europe Digit. Days; Int. Exhib. Conf. Power Electron. Intell. Motion Renewable Energy Energy Manage.*, 2021, pp. 1–8.
[145] S. Takahashi and S. Maekawa, "Wideband small-signal model of common-mode inductors based on stray capacitance estimation method," *IEEJ J. Ind. Appl.*, vol. 11, no. 3, pp. 514–521, Nov. 2022.
[146] S. Wang, F. C. Lee, D. Y. Chen, and W. G. Odendaal, "Effects of parasitic parameters on EMI filter performance," *IEEE Trans. Power Electron.*, vol. 19, no. 3, pp. 869–877, May 2004.
[147] H. Chen, Z. Qian, Z. Zeng, and C. Wolf, "Modeling of parasitic inductive couplings in a pi-shaped common mode EMI filter," *IEEE Trans. Electromagn. Compat.*, vol. 50, no. 1, pp. 71–79, Feb. 2008.
[148] H. Li, C. Feng, Z. Yang, and Z. Yang, "An improved ferrite choke RLC model and its parameters determination method," in *Proc. 43rd Annu. Conf. IEEE Ind. Electron. Soc.*, 2017, pp. 6995–6999.
[149] L. Dehong and J. Xanguo, "High frequency model of common mode inductor for EMI analysis based on measurements," in *Proc. 3rd Int. Symp. Electromagn. Compat.*, 2002, pp. 462–465.
[150] I. Stevanović and S. Skibin, "Behavioral circuit modeling of single-and three-phase chokes for EMI simulations," in *Proc. Int. Power Electron. Conf.*, 2010, pp. 2867–2871.
[151] C. Dominguez-Palacios, J. Bernal, and M. Prats, "Characterization of common mode chokes at high frequencies with simple measurements," *IEEE Trans. Power Electron.*, vol. 33, no. 5, pp. 3975–3987, May 2018.
[152] W. Tan, C. Cuellar, X. Margueron, and N. Idir, "A high frequency equivalent circuit and parameter extraction procedure for common mode choke in the EMI filter," *IEEE Trans. Power Electron.*, vol. 28, no. 3, pp. 1157–1166, Mar. 2013.
[153] Z. Li et al., "Parameter extraction for equivalent circuit of common mode choke based on deep neural network, random forest tree and extreme gradient boosting algorithm," in *Proc. Photon. Electromagn. Res. Symp. Fall*, 2019, pp. 2296–2304.
[154] C. Dominguez-Palacios, J. B. Mendez, and M. A. M. Prats, "Characterization of three-phase common-mode chokes at high frequencies," *IEEE Trans. Power Electron.*, vol. 33, no. 8, pp. 6471–6475, Aug. 2018.
[155] H. Chen and Z. Qian, "Modeling and characterization of parasitic inductive coupling effects on differential-mode EMI performance of a boost converter," *IEEE Trans. Electromagn. Compat.*, vol. 53, no. 4, pp. 1072–1080, Nov. 2011.
[156] W. Chen, L. Feng, H. Chen, and Z. Qian, "Near field coupling effects on conducted EMI in power converter," in *Proc. IEEE Power Electron. Spec. Conf.*, 2006, pp. 1–6.
[157] H. Zhu, D. Liu, H. Chen, and G. Chen, "An improved foster model of common-mode inductor and its application in EMI filter design," in *Proc. IEEE Joint Int. Symp. Electromagn. Compat. Asia–Pacific Int. Symp. Electromagn. Compat.*, 2018, pp. 461–465.
[158] H. Chen, Y. Hu, L. Wang, Z. Zhang, and G. Chen, "EMI filter design based on high-frequency modeling of common-mode chokes," in *Proc. IEEE 27th Int. Symp. Ind. Electron.*, 2018, pp. 384–388.
[159] Z. Pan et al., "An equivalent modeling method of passive components with multi-resonant frequency," *Int. J. Circuit Theory Appl.*, vol. 51, no. 6, pp. 2689–2704, Feb. 2023.
[160] I. Stevanović and S. Skibin, "Behavioral circuit modeling of single-and three-phase chokes with multi-resonances," in *Proc. Int. Conf. Power Electron.*, 2011, pp. 435–439.
[161] S. Skibin and I. Stevanović, "Behavioral circuit modeling of chokes with multi-resonances using genetic algorithm," in *Proc. IEEE Int. Symp. Electromagn. Compat.*, 2011, pp. 454–458.
[162] S. Huang, K. Y. See, F. Fan, R. Simanjorang, and F. Sasongko, "Behavioural modeling of common-mode chokes with frequency-dependent permeability core," in *Proc. Asia-Pacific Int. Symp. Electromagn. Compat.*, 2021, pp. 1–4.
[163] S. Takahashi and S. Ogasawara, "A novel simulation model for common-mode inductors based on permeance-capacitance analogy," in *Proc. IEEE Energy Convers. Cong. Expo.*, 2020, pp. 5862–5869.
[164] A. Ojeda-Rodríguez, C. Dominguez-Palacíos, J. Bernal-Méndez, and M. Martín-Prats, "Simple and accurate characterization of nanocrystalline common mode chokes," in *Proc. IEEE Int. Symp. Electromagn. Compat. Signal/Power Integr.*, Aug. 2022, pp. 472–477.
[165] L. Dalessandro, F. da Silveira Cavalcante, and J. W. Kolar, "Self-capacitance of high-voltage transformers," *IEEE Trans. Power Electron.*, vol. 22, no. 5, pp. 2081–2092, Sep. 2007.
[166] S. F. Zarei and S. Khankalantary, "A simplified frequency model for industrial common-mode chocks used in high-power converters," *J. Electromagn. Eng. Sci.*, vol. 21, no. 1, pp. 15–22, Jan. 2021.
[167] K. Nomura, N. Kikuchi, Y. Watanabe, S. Inoue, and Y. Hattori, "Novel SPICE model for common mode choke including complex permeability," in *Proc. IEEE Appl. Power Electron. Conf. Expo.*, Long Beach, CA, USA, 2016, pp. 3146–3152.
[168] M. Illia, L. Koleff, and G. Griepentrog, "Non-ideal model of the common mode choke for EMI filters," in *Proc. IEEE Appl. Power Electron. Conf. Expo.*, 2017, pp. 938–944.
[169] "SPICE-A brief tutorial," Univ. of Pennsylvania, 2010. [Online] Available: https://www.seas.upenn.edu/~jan/spice/spice.overview.html
[170] C. Cuellar, N. Idir, and A. Benabou, "High-frequency behavioral ring core inductor model," *IEEE Trans. Power Electron.*, vol. 31, no. 5, pp. 3763–3772, May 2016.
[171] C. Cuellar, A. Benabou, and N. Idir, "High frequency model of ferrite and nanocrystalline ring core inductors," in *Proc. 17th Eur. Conf. Power Electron. Appl.*, 2015, pp. 1–8.
[172] A. M. Sanchez, A. Pérez, J. R. Regué, M. Ribó, P. Rodríguez-Cepeda, and F. J. Pajares, "A modal model of common-mode chokes for conducted interference prediction," *IEEE Trans. Electromagn. Compat.*, vol. 52, no. 3, pp. 749–752, Aug. 2010.
[173] C. Dominguez-Palacios, P. González-Vizuete, and J. B. Escuela, "Effect of conducting surfaces on the performance of common mode chokes," in *Proc. IEEE Int. Symp. Electromagn. Compat. IEEE Asia-Pacific Symp. Electromagn. Compat.*, 2018, pp. 363–368.

[174] "Radio disturbance characteristics for the protection of receivers used on board vehicles, boats and on devices-limits and methods of measurement, British standards," London, U.K., 2008. [Online]. Available: https://bsol.bsigroup.com
[175] I. Grobler and M. Gitau, "Characterising and modelling extended conducted electromagnetic emission," in *Proc. IEEE ECCE Asia Downunder*, 2013, pp. 1131–1136.
[176] Z. Ma, S. Wang, H. Sheng, and S. Lakshmikanthan, "Modeling, analysis and mitigation of radiated EMI due to PCB ground impedance in a 65W high-density active-clamp flyback converter," *IEEE Trans. Ind. Electron.*, vol. 70, no. 12, pp. 12267–12277, Dec. 2023.
[177] J. Yao, Z. Ma, Y. Lai, and S. Wang, "A survey of modeling and reduction techniques of radiated EMI in power electronics," in *Proc. IEEE Int. Joint EMC/SI/PI EMC Eur. Symp.*, 2021, pp. 1081–1086.
[178] Z. Ma et al., "Radiated EMI prediction in power converters with power cables based on cable antenna voltage gain extraction," in *Proc. IEEE Int. Symp. Electromagn. Compat. Signal/Power Integr.*, 2022, pp. 510–515.
[179] X. Zhao et al., "Planar common-mode EMI filter design and optimization for high-altitude 100-kW SiC inverter/rectifier system," *IEEE J. Emerg. Sel. Topics Power Electron.*, vol. 10, no. 5, pp. 5290–5303, Oct. 2022.
[180] W. Su, H. Li, C. Ji, Z. Wang, X. Liu, and B. Zhang, "High-frequency aging model modeling method of passive devices in EMI filter based on electromagnetic field analysis," *IEEE Trans. Power Electron.*, vol. 38, no. 12, pp. 15535–15550, Dec. 2023.
[181] R. Suárez, M. Tijero, R. Moreno, and J. M. González, "Modeling methodology of magnetic toroidal cores for 3-D FEM full-wave simulation up to 100 MHz," *IEEE Trans. Power Electron.*, vol. 39, no. 8, pp. 9638–9649, Oct. 2024.
[182] J. Borsalani, A. Dastfan, and J. Ghalibafan, "An integrated EMI choke with improved DM inductance," *IEEE Trans. Power Electron.*, vol. 36, no. 2, pp. 1646–1658, Feb. 2021.
[183] P. Ruiz-Morales, Á. Ojeda-Rodríguez, J. Bernal-Méndez, and M. A. Martín-Prats, "Winding optimization for reducing parasitic capacitances of common-mode chokes," *IEEE Trans. Electromagn. Compat.*, vol. 66, no. 4, pp. 1125–1135, Aug. 2024.
[184] S. Wang and F. C. Lee, "Analysis and applications of parasitic capacitance cancellation techniques for EMI suppression," *IEEE Trans. Ind. Electron.*, vol. 57, no. 9, pp. 3109–3117, Sep. 2010.
[185] H. Huang and T. Lu, "A cancelation method of mutual inductance between capacitors in EMI filter," *IEEE Trans. Power Electron.*, vol. 37, no. 10, pp. 11974–11984, Oct. 2022.
[186] H. Chen and S. Ye, "Modeling and optimization of EMI filter by using artificial neural network," *IEEE Trans. Electromagn. Compat.*, vol. 61, no. 6, pp. 1979–1987, Dec. 2019.
[187] H. Hackl, M. Stoiber, B. Auinger, T. Zengerle, F. Königseder, and J. Hansen, "Python-LTSpice framework for multi-objective EMC filter optimization," in *Proc. Int. Symp. Electromagn. Compat.*, 2023, pp. 1–6.
[188] X. Li, Y. Liu, J. Yang, and X. Wu, "Decoupled magnetic integration of symmetrical LCL filter with a common-mode inductor for single-phase grid-connected converters," *IEEE J. Emerg. Sel. Topics Power Electron.*, vol. 3, no. 4, pp. 966–977, Oct. 2022.
[189] S. Jiang, W. Wang, P. Wang, and D. Xu, "A fully integrated common-mode choke design embedded with differential-mode capacitances," *IEEE Trans. Power Electron.*, vol. 37, no. 5, pp. 5501–5513, May 2022.
[190] Y. Yan, J. Moss, K. D. Ngo, Y. Mei, and G.-Q. Lu, "Additive manufacturing of toroid inductor for power electronics applications," *IEEE Trans. Ind. Appl.*, vol. 53, no. 6, pp. 5709–5714, Nov./Dec. 2017.

Huamin Jie (Graduate Student Member, IEEE) received the B.Eng. degree in electrical engineering from Wuhan University, China, in 2019, and the M.Sc. degree in power engineering from Nanyang Technological University (NTU), Singapore, in 2020. He is currently working toward the Ph.D. degree in electrical engineering with NTU.

His research interests include device modeling, electromagnetic interference (EMI), EMI filter design, fault detection, impedance measurement, intentional EMI, and power converter systems.

Dr. Jie was a recipient of the Best Paper Awards at the 2022 Asia-Pacific International Symposium on Electromagnetic Compatibility and the 2023 International Conference on Sensing, Measurement, Communication, and Internet of Things Technologies.

Zhenyu Zhao (Senior Member, IEEE) received the B.Eng. degree in electrical engineering from the Huazhong University of Science and Technology, Wuhan, China, in 2015, and the Ph.D. degree in electrical engineering from Nanyang Technological University (NTU), Singapore, in 2021.

From 2021 to 2023, he was a Research Fellow with NTU and concurrently served as the Director of EEE-RSA. He is currently a Lecturer with the Department of Electrical and Computer Engineering, National University of Singapore. His research interests include electromagnetic compatibility (EMC), electromagnetic technologies, modern transportation, impedance measurement and modeling, etc. He has authored or coauthored 1 book, more than 50 journal articles, 40 conference papers, and granted 2 international patents.

Dr. Zhao was a recipient of more than ten prestigious awards from various international societies, journals, and conferences, including the Best Student Paper Award from the Joint IEEE International Symposium on EMC and Asia-Pacific International Symposium on EMC (Joint IEEE EMC and APEMC) in 2018, the Young Scientist Award and the Best Paper Award from APEMC in 2022, the Young Scientist Award from the International Union of Radio Science in 2023, the Emerging Leader Award from *Measurement Science and Technology* in 2024, the Young Professional Ambassador from the IEEE EMC Society in 2024–2025, etc. He has served in executive positions at various international conferences, such as the TPC Chair of APEMC in 2026, Publicity Chair of SWA in 2024, and Tutorial Instructor of I2MTC in 2023. He also serves as an Associate Editor for *Measurement*, IEEE TRANSACTIONS ON VEHICULAR TECHNOLOGY, *IET Science, Measurement and Technology*, and *Chinese Journal of Electrical Engineering*; the Lead/Executive Guest Editor for *Measurement* and *IET Power Electronics*. He has been the Chair of the IEEE EMC Society Singapore Chapter since 2024.

Hong Li (Senior Member, IEEE) received the B.E. degree in electrical engineering from the Taiyuan University of Technology, Taiyuan, China, in 2002, the M.E. degree in electrical engineering from the South China University of Technology, Guangzhou, China, in 2005, and the Ph.D. degree in electrical engineering from Fern Universität in Hagen, Hagen, Germany, in 2009.

She is a Full Professor with the College of Electrical Engineering, Zhejiang University, China. She has authored/coauthored 1 book, 40 journal papers, and 45 conference papers. She has granted more than 20 patents. Her research interests include nonlinear modeling, analysis, and its applications, electromagnetic interference suppressing methods for power electronic systems, and widebandgap power devices and applications.

Prof. Li is an Associate Editor for IEEE TRANSACTIONS OF INDUSTRIAL ELECTRONICS, IEEE OPEN JOURNAL OF INDUSTRIAL ELECTRONICS SOCIETY, and *Chinese Journal of Electrical Engineering* and the Vice Chairman of the Electromagnetic Compatibility Specialized Committee in China Power Supply Society.

Changdong Wang (Member, IEEE) was born in 1995. He received the B.Eng. degree in mechanical engineering and automation from the Heilongjiang University, Harbin, China, the M.Sc. degree in mechanical engineering from North Eastern University, Shenyang, China, in 2021. He is currently working toward the Ph.D. degree in information and communication engineering in Harbin Institute of Technology, Harbin, China.

He was a visiting student with Oxford University. His research interests include deep learning, signal processing, fault diagnosis, and power electronics.

Yongqi Chang (Graduate Student Member, IEEE) received the B.Eng. and M.Eng. degrees in instrument science and engineering in 2018 and 2020, respectively, from the Harbin Institute of Technology, Harbin, China, where he is currently working toward the Ph.D. degree in control science and engineering.

His research interests include rail crack detection, electromagnetic applications, fault diagnosis, and structural health monitoring.

Kye Yak See (Senior Member, IEEE) received the B.Eng. degree in electrical engineering from the National University of Singapore, Singapore, in 1986, and the Ph.D. degree in electrical engineering from Imperial College London, London, U.K., in 1997.

From 1986 to 1991, he was with Singapore Technologies Electronics, Singapore, as a Senior Engineer. From 1991 to 1994, he was a lead Design Engineer with ASTEC Custom Power, Singapore. Since 1997, he has been with Nanyang Technological University (NTU), Singapore, as a Faculty Member. He is currently an Associate Professor with the School of Electrical and Electronic Engineering, NTU. He holds a concurrent appointment as the Director of the Electromagnetic Effects Research Laboratory. His current research interests are electromagnetic compatibility (EMC), signal integrity and real-time condition monitoring. He has been the Managing Editor for the IEEE EMC MAGAZINE since 2011 and an Associate Editor for the IEEE TRANSACTIONS ON EMC since 2024.

Dr. See was a recipient of the 2021 National Day's Public Administration Medal (Bronze) Award from Singapore's Prime Minister Office for his technical achievements and contributions toward the greater good of Singapore society.